PETROLOGY AND GEOCHEMISTRY OF A TUFFACEOUS SUITE, HEMLO AREA, ONTARIO

PETROLOGY AND GEOCHEMISTRY OF THE TUFFACEOUS FOOTWALL ROCKS OF THE WILLIAMS ORE ZONE, HEMLO AREA ONTARIO

By

Douglas G. McIlveen

Submitted to the Department of Geology
in Partial Fulfilment of the Requirements for
the Degree Bachelor of Science

McMaster University

April, 1983

BACHELOR OF SCIENCE (1983)
(Geology)

McMASTER UNIVERSITY
Hamilton, Ontario

TITLE: Petrology and Geochemistry of the Tuffaceous Footwall Rocks of the Williams Ore Zone, Hemlo Area, Ontario.

AUTHOR: Douglas G. McIlveen

SUPERVISOR: Dr. H.D. Grundy

NUMBER OF PAGES: ix, 93

ABSTRACT

The recent discovery of ore grade gold in the Hemlo area of Northern Ontario has provided the initiative for extensive exploration in that region. This study concentrates on rocks from the footwall to the ore zone on the Williams property of Long Lac Mineral Exploration.

The footwall rocks consist of fine grained, finely laminated tuffs. The suite has undergone low grade regional metamorphism. Retrograde metamorphic effects are also present but appear to be confined to certain bands. Some of the minerals may have been introduced by the action of metasomatic fluids.

The tuffs are quite felsic and many have the composition of a rhyolite. Samples tested for gold have up to 200 times the background concentration of a rhyolite. The gold is associated with high SiO_2 and K_2O and low Al_2O_3, CaO, Na_2O, Fe_2O_3 and MgO contents.

The ore deposit is similar in many respects to the Bousquet deposit of Northern Quebec. The Bousquet deposit has been interpreted as syngenetic by some authors and therefore it is quite possible that the Hemlo deposit is syngenetic as well. However the metamorphism and possible metasomatism that these rocks have undergone suggests that it may be an

epigenetic deposit. Due to the limited number of samples in this study it could not conclusively be determined which hypothesis is correct.

ACKNOWLEDGEMENTS

The author is indebted to Mr. G. Smith and Mr. B. Valliant who convinced me to write this thesis. Long Lac Mineral Exploration is thanked for providing the funds for XRF data.

The advice and constructive criticism from my superviser, Dr. H.D. Grundy was appreciated. The help of J.A. Fyon and M. Lavigne was instrumental in completing this thesis and I cannot thank them enough.

Mr. A. Kabir is thanked for his time in helping with the process of instrumental neutron activation anlaysis. Mr. L. Zwicker is thanked for locking himself in the basement and cutting the thin sections. Mr. J. Whorwood is thanked for providing his photographic expertise. The typing of the manuscript was undertaken by Mrs. H. Kennelly on last minute notice and this was very much appreciated.

The bulk of my gratitude is saved for Ms. Kelly Acker who helped to edit the manuscript and got the author through the year in one piece.

TABLE OF CONTENTS

LIST OF FIGURES

LIST OF PLATES

LIST OF TABLES

CHAPTER 1

INTRODUCTION

The Hemlo area, covering an area of some 415 km^2 within the District of Thunder Bay, is located approximately 350 km east of Thunder Bay via the Trans-Canada highway (Muir, 1980). here has recently been a flurry of activity in this area due to the discovery of ore-grade gold. The samples upon which this study is based, however, represent the footwall and do not contain mineable amounts of gold.

1.1 LOCATION

Samples were collected, by the author, in the summer of 1982 while working for Long Lac Mineral Explorations Ltd. The property from where they were taken is known as the Williams Claim Group (Fig. 1.1). This group, consisting of eleven claims, is located approximately half-way between the towns of White River and Marathon, Ontario. Part of the southern boundary of the property is the Trans-Canada highway which provides good access.

1.2 PREVIOUS GEOLOGICAL WORK

The earliest reported mapping in the Hemlo area was done by J.E. Thompson in 1930 (Muir, 1982). This, however, only covered part of the Hemlo area since the main area he mapped was further west. In 1957 a geological report was assembled

Fig. 1.1 Map of Williams Claim Group showing study area and drill hole location.

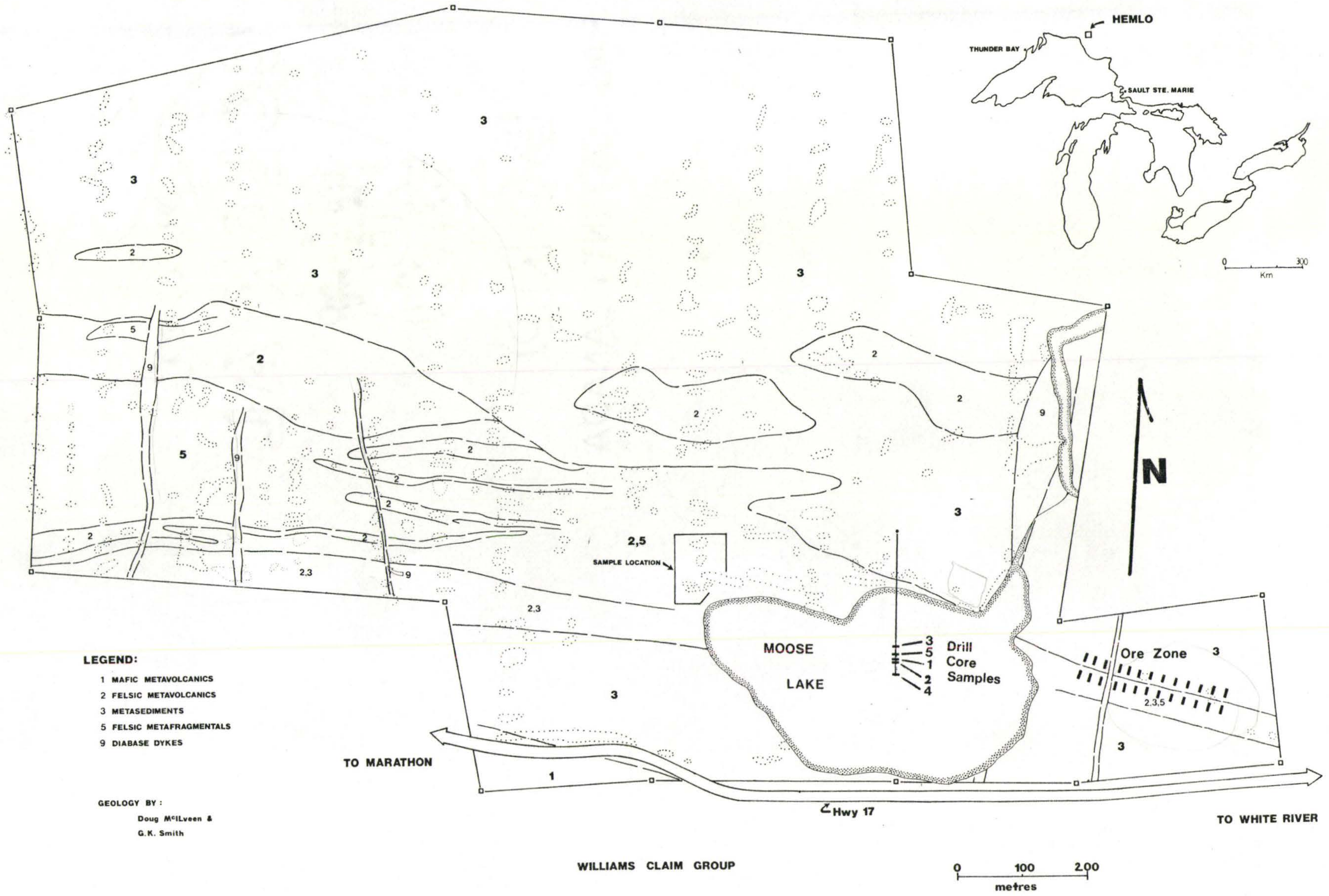

WILLIAMS CLAIM GROUP

for the Canadian PAcific Railway which encompassed the Hemlo area as well as large tracts of land to the North and the East. (Bartley and Page, 1957). Due to the expansive area covered this was a very general report. Compilation maps that included the Hemlo area were issued by the Ontario government in 1968, 1969 and 1972 (Muir, 1982). The most extensive mapping of the entire Hemlo area was carried out by Muir, et. al. (Muir, 1982) for the Ontario Geological Survey in the summer of 1978,

1.3 PREVIOUS EXPLORATION

Early exploration in the area was centred in the Williams Claim Group area. The property was first staked in 1945 after gold showings were reported in the vicinity. A drilling program initiated at this time did not indicate high enough gold values to prompt further work.

Interest in the Williams Clark Group was rekindled with the discovery in 1981, by International Corona Resources Ltd., of two zones of gold mineralization on an adjacent property immediately to the east. By August, 1982, after an extensive drilling program, Long Lac Mineral Exploration was able to announce the discovery of an ore body on the Williams property.

1.4 GENERAL GEOLOGY

The Hemlo area is part of the Eastern extension of the Schreiber-Marathon belt, which is a small Archean greenstone belt. The dominant rock types are a series of interfingering mafic lava flows and associated mafic pyroclastics, intermediate to felsic volcanics (largely pyroclastics) and associated thin to thickly bedded sediments. Metamorphism of these rocks tends to be regional low grade but locally can reach up to medium grade (Muir, 1982). Large granitic plutons, with associated gneissic assemblages, as well as mafic to felsic dykes and sills are also common rock types of the Helmo area.

Relief over the area as a whole is generally moderate but ranges from as much as 230 m on steep sided hills to practically zero in flat lying swampy areas (Muir, 1982). Outcrop exposure is very good in areas of higher relief.

The Williams property itself is an area of varied relief ranging from moderate to practically nil. The highest relief is attained in the North-east sector where steep cliffs up to 30 m high are present. The lowest relief is found in the middle of the Western end of the property where swampy conditions prevail. Outcrop exposure is usually good but in areas between outcrops the overburden is thick.

There is little in the way of mafic volcanics and there are no granitic nor gneissic rocks on the Williams Claim Group. The main rock types represented are metasediments and intermediate to felsic pyroclastics. On the Eastern side of the property the average strike is approximately 290° while on the Western side it is closer to 275°. The dip measures between 65° and 70° to the north. The metasediments and pyroclastics often share similar characteristics which tends to make field mapping a problem. Felsic porphyritic sills, as well as mafic dikes and sills commonly cut the matasedimentary and pyroclastic units.

1.5 METHODOLOGY

The samples obtained are of the same stratigraphic unit that make up the footwall sequence of the orebody. The sample location is approximately 700 m west of the orebody (Fig. 1.1). Outcrop exposure was particularly good in this area since it was on the side of a hill.

Samples A through J were extracted from six separate outcrops over a North-South distance of about 45 m. The outcrops were mapped using a North-South cut line which had been part of a grid system used for mapping in the summer (Fig. 1.2).

The rocks make up an intermediate to felsic tuffaceous assemblage. Sample A is a finely laminated intermediate tuff which forms the base of the sequence. It weathers a medium grey colour. Above this lies the unit from which samples C, D and E were taken. It is a finely laminated felsic tuff and it weathers a light brown. The upper limit of the tuffaceous assemblage is represented by samples F, G and H. It is a 'massive' felsic tuff with very weak laminations. This unit weathers a rusty brown and has undergone more extensive weathering at its top (Sample H) than at its base (sample F).

Two mafic sills (samples B and I) and a quartz and feldspar porphyritic sill (sample J) were also taken from the area.

Fig. 1.2 Detail of sample location on Williams Property.

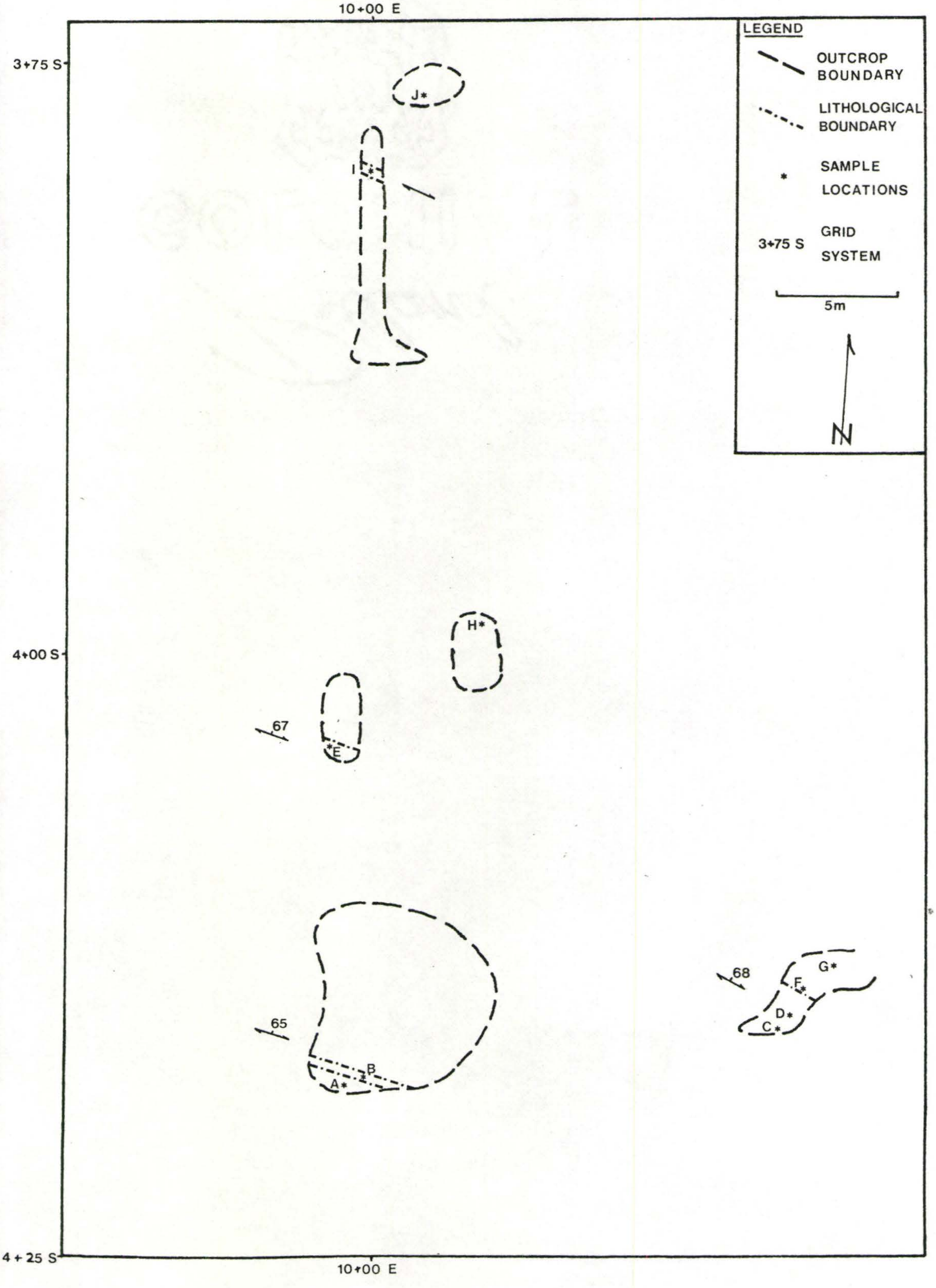
10+00 E
3+75 S
4+00 S
4+25 S
10+00 E
LEGEND
OUTCROP BOUNDARY
LITHOLOGICAL BOUNDARY
SAMPLE LOCATIONS
3+75 S GRID SYSTEM
5m
N
J
I
H
E
67
65
68
A
B
C
D
F
G

Pieces of core, from a drill hole further to the East (Fig. 1.1), were obtained from Long Lac Mineral Exploration Ltd. Core samples 1, 2, 3A, 4 and 5 appear to be related to the felsic tuffaceous units already described while sample 3B is a feldspar porphyritic sill. The core was taken from drill hole W5 at depths of 214.5 m for samples 3A and 3B, 220.5 m for sample 5, 230 m for sample 1, 233.5 m for sample 2 and 262.5 m for sample 4.

Thin sections were cut from the ten hand specimens and from six pieces of core for a total of sixteen samples. A thorough mineralogical and textural description of each section was then carried out. Some minerals could not be identified by traditional petrographic methods but this problem was resolved by using x-ray diffraction techniques.

Whole rock analyses of ten major oxides were obtained for fifteen samples (all except E), using x-ray fluorescence. The concentration of gold was determined for nine samples by using Instrumental Neutron Activation Analysis. The geochemical information was used to classify the rocks and to determine variations in the major oxides relative to gold.

CHAPTER 2

METAMORPHISM

2.1 TEXTURES

Metamorphic textures are prevalent in these rocks and include undulose extinction in quartz and sutured grain boundaries within porphyroblasts of quartz. Not all of the textures are fully understood but they are interpreted to be metamorphic.

Undulose or strained extinction was observed in quartz of all the sections. It is the result of permanent bending of crystal lattices due to high strain (Spry, 1979).

Polygonal crystallization of the quartzo-feldspathic groundmass was noted in the majority of thin sections. It was especially prominent in sections F, G and H (Plate 2.1). This is a process that reduces the grain boundary tension of a polycrystalline aggregate. In metamorphic rocks each grain fits together with its neighbour to fill space with no voids and adopts a polyhedron that has the smallest surface area for a given volume. The shape of this polyhedron is a truncated octahedron, consisting of fourteen sides (Hobbs, et al., 1976).

Platey minerals as well as tourmaline consistently had a parallel or subparallel alignment which gave many of the units a strong schistosity.

In samples C, D, E, 1 and 2 the parallel alignment of platey minerals and tourmaline was obvious but a distinct continuous banding, differentiating the quartzo-feldspathic and

Plate 2.1 Photomicrograph of polygonal crystallization of microcline and quartz from thin section G. Cross nicols. Magnification is 160×.

Plate 2.2 Photomicrograph of thin section D showing general foliation and distribution of quartz porphyroblasts. Plane polarized light. Magnification is 5.0×.

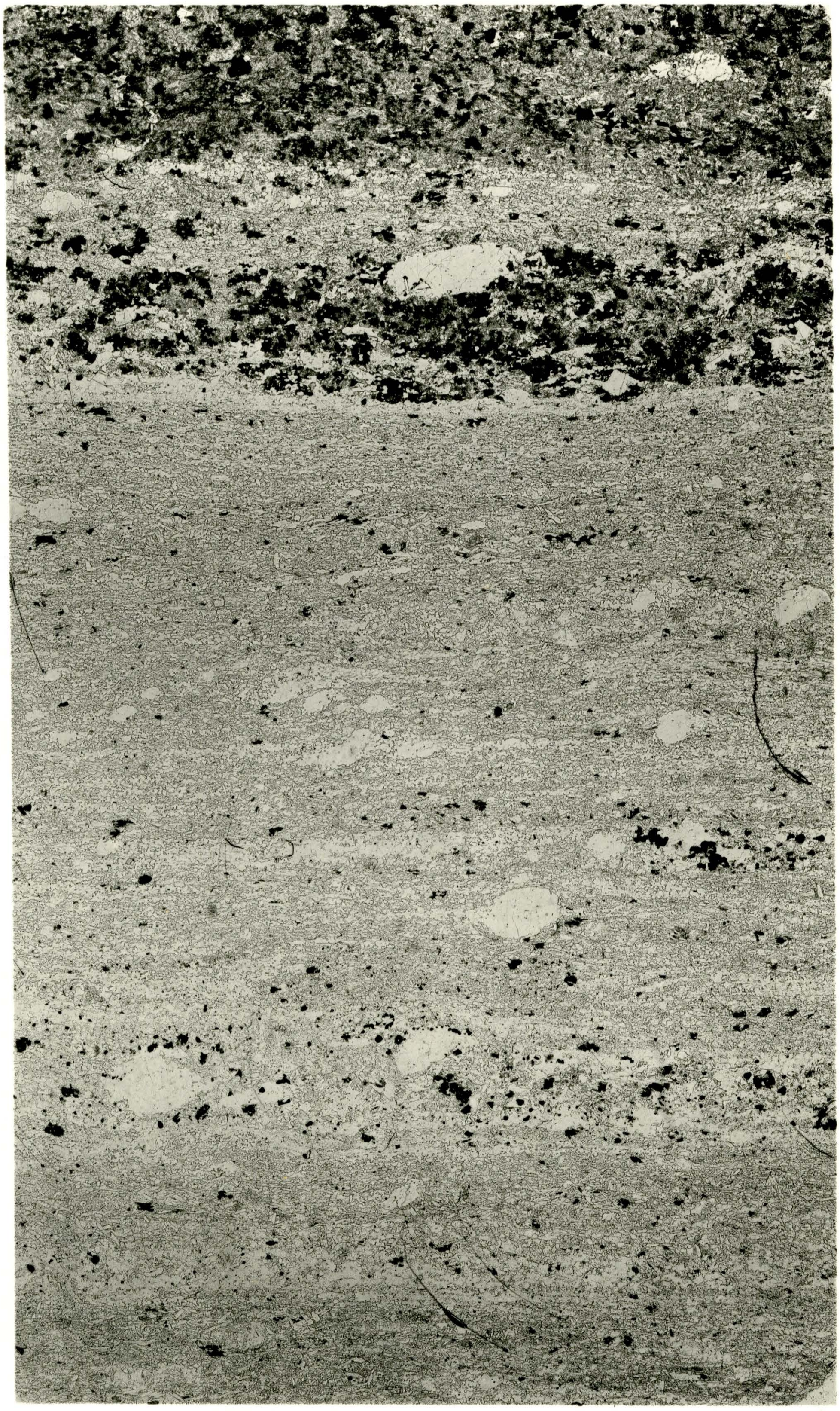

Plate 2.3 Photomicrograph of thin section D showing strong schistocity and alternating bands of quartzo-feldsphatic and micaceous material. Cross nicols. Magnification is 5.0×.

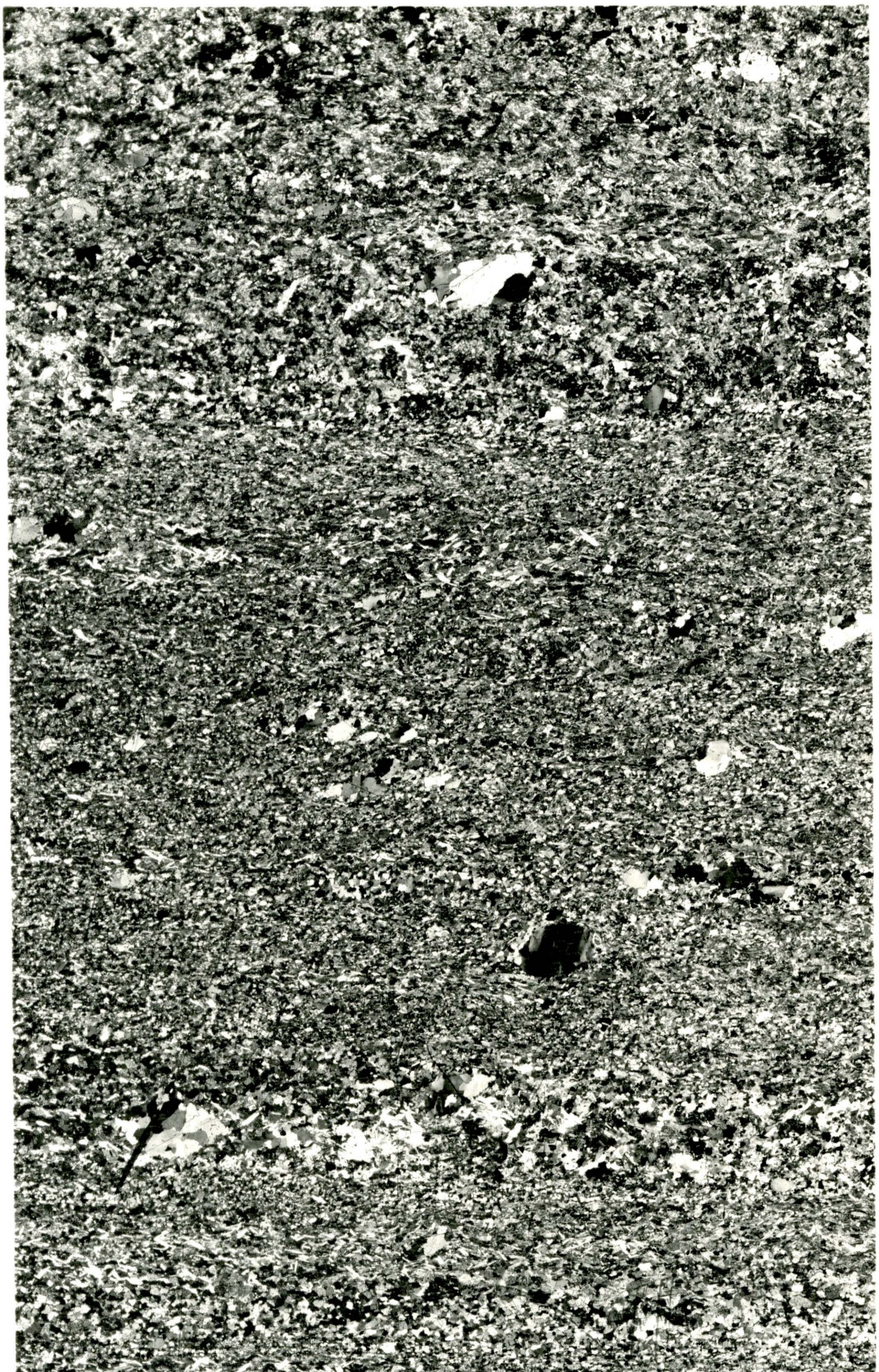

Plate 2.4 Photomicrograph of a quartz porphyroblast from thin section D. Note elongation parallel to foliation. Cross nicols. Magnification is 25×.

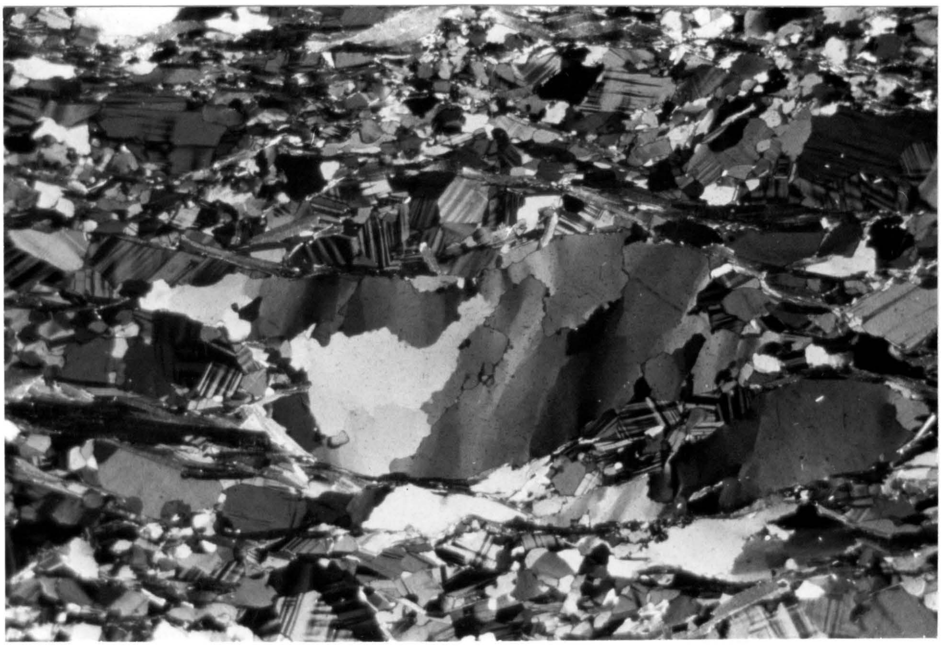

the platey minerals, was also evident. The banding is best represented by sample D which is the least weathered of the three rocks (C, D and E) representing the finely laminated felsic tuff unit (Plate 2.2 and 2.3). The width of each individual band was usually on the order of 1.0 to 2.0 m.

Another important constituent of all the felsic tuffaceous units, whether they were schiotose or 'massive', was porphyroblasts of quartz (Plate 2.4). They were not noted in any of the sills except for section J. However in this section the quartz aggregates would be better termed phenocrysts as they appear to be of igneous origin.

In each section the porphyroblasts were usually elongated parallel to each other. In the schistose felsic units they were elongated parallel to the platey elements. At the same time the platey minerals were noted to bend around the porphyroblasts.

It is possible that the grains are ejecta from felsic volcanism (Spry, 1979) but this is doubtful since, if this was the case, one would expect to see the development of pressure shadows but they do not seem to be present. On the other hand the porphyroblasts must have been present before regional metamorphism overprinted the assemblage since platey minerals often bend around them.

The porphyroblasts often have subgrains. The boundaries between these subgrains are usually sutured (Plate 2.5) while quartzo-feldspathic material in the surrounding groundmass

Plate 2.5 This photomicrograph shows a close up of a quartz porphyroblast from sample 2. Note subgrains with sutured grain boundaries and mica bending around the porphyroblast. Cross nicols. Magnification is 63×.

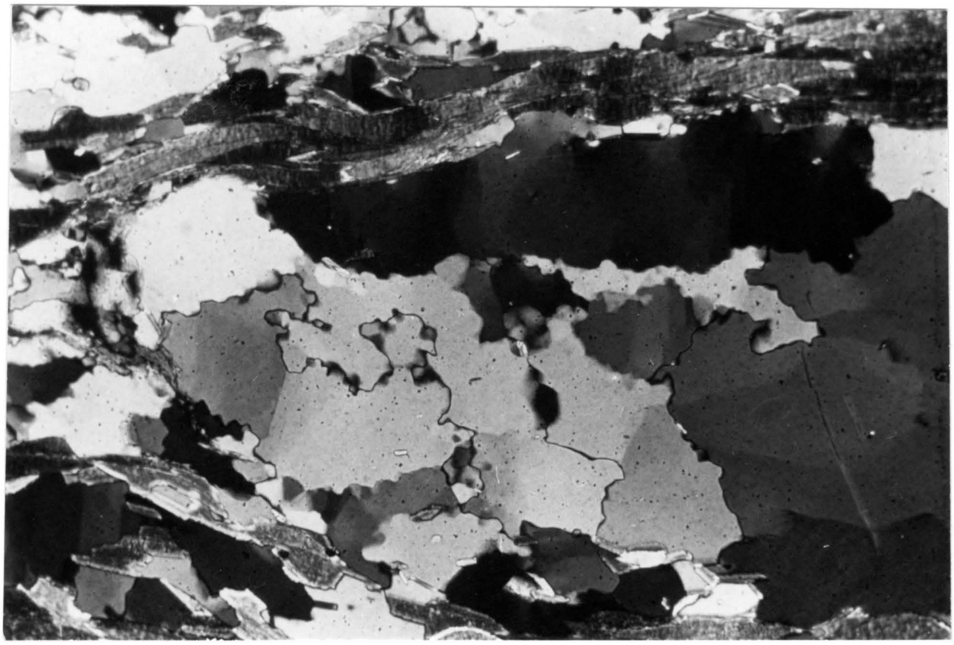

is polygonalized. The origin of sutured grain boundaries is not well understood but they may represent a "frozen" image of a non-equilibrium boundary produced during metamorphic recrystallization (Spry, 1979). Therefore it is very possible that these quartz aggregates represent recrystallization during metamorphism and hence the term porphyroblast is appropriate.

It is interesting to note that polycrystalline quartz clasts have been described in the tuffaceous footwall rocks of the Agnico-Eagle gold deposit in Quebec (Barnett, et al., 1982). He has interpreted these as original chert which has recrystallized.

2.2 METAMORPHIC GRADE

The equilibrium assemblage was determined for the felsic tuffaceous units. Minerals were considered to be in equilibrium when they displayed metamorphic textures such as polygonal crystallization or when two different minerals shared a common boundary without showing obvious replacement of one by the other.

Two equilibrium assemblages were determined for these rocks, one being almandine garnet + biotite + chlorite + quartz + muscovite and the other being chlorite + biotite + K-feldspar + quartz + muscovite. Even though the garnet was a very minor component tiny crystals were present in many of the sections so it was included in the equilibrium assemblage.

The assemblages were plotted on an AFM diagram (Fig. 2.1) (Winkler, 1979). The diagram indicates that the equilibrium assemblages are part of the [almandine]-low grade or almandine + quartz + muscovite zone. Therefore these results compare favourably with the results of Muir (1980) who found the dominant metamorphism of the Hemlo area to be regional low grade.

Fig. 2.1 AFM diagram plotting equilibrium assemblages seen in the tuffaceous units.

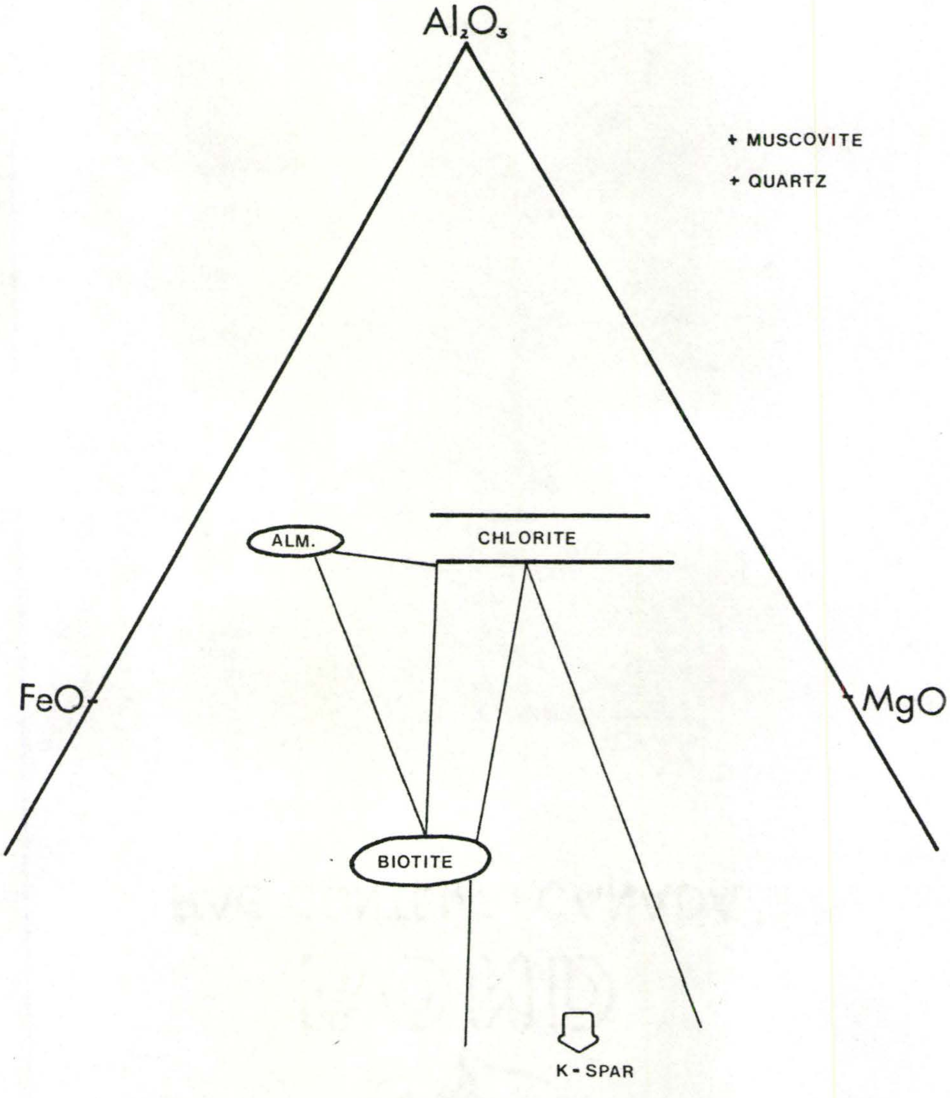
Al_2O_3
+ MUSCOVITE
+ QUARTZ
CHLORITE
ALM.
FeO
MgO
BIOTITE
K - SPAR

CHAPTER 3

METASOMATISM AND RETROGRADE METAMORPHISM

3.1 XRD MINERAL IDENTIFICATION

Trouble was encountered in trying to identify some of the minerals in the thin sections. Minerals that could not be identified using the microscope were determined by using x-ray diffraction (XRD). The Gandolfi camera method was used (Berry and Mason, 1959). The radius of the camera was 57.3 mm and the film used was Kodak, no-screen, x-ray film.

3.1.1 METHOD OF ANALYSIS

Once a mineral was determined to be unidentifiable by conventional means the cover slip was taken off the thin section and the unknown mineral was removed with the use of a needle. The mineral was then mounted on the tip of a glass fibre which was then placed inside the camera.

The camera was, in turn, set up on the XRD apparatus and a beam of CuKα x-radiation was directed through the camera at the mineral. At the same time the mineral was slowly rotated by an electric motor to randomize its orientation. The d-spacings of the mineral caused the beam to scatter and this scattering formed darkened rings on the film.

The diameter of a ring was 2θ and this was measured using a millimeter scale. This could then be substituted into the Bragg equation ($\lambda = 2\delta\sin\theta$, where $\lambda = 1.54178$) and hence the δ-spacings of the mineral could be obtained.

To identify each mineral the δ-spacing of the most intense ring was first determined and matched in the search manual (Joint Committee on Powder Diffraction Standards, 1980). Further δ-spacings of less intense rings were then matched until a best fit could be obtained.

A pattern was then taken for this "best fit" mineral, again using the Gandolfi camera. The two films were then compared to see if they were the same mineral.

3.1.2 MINERALS IDENTIFIED

The Gandolfi camera facilitated the identification of analcime, barite, heulandite, rutile and tourmaline. The tables on the following pages (Tables 3.1-3.5) show how the calculated δ-spacings match up with those listed in the Search Manual. For the calculated δ-spacings the rings are numbered as a function of decreasing strength. Less clear rings are listed as weak (w) and very weak (vw). In the search manual column the higher numbers represent the most intense rings.

3.2 METASOMATISM

In a major study of the abundance of gold in common rocks it was noted that the highest gold values were obtained from rocks which showed the effects of metasomatism (Crocket, 1978). There is reason to believe that the tuffaceous assemblage, which is the subject of this thesis, has undergone metasomatism.

Tables 3.1 and 3.2: Tables compare data obtained using the Gandolfi camera with values from experimental powder diffraction data for dravite and barite, respectively.

GANDOLFI CAMERA DATA

Order of Intensity	2θ	δ-spacing
3	21.15	4.20
4	22.40	3.97
vw	25.60	3.42
1	26.80	3.33
6	30.28	2.95
2	34.80	2.58
5	44.40	2.04
w	47.20	1.93
w	50.20	1.82
w	55.35	1.66
w	57.70	1.60

DATA FROM POWDER DIFFRACTION TABLES FOR DRAVITE

Intensity	δ-spacing
65	4.220
85	3.990
60	3.480
100	*3.343
85	2.961
100	2.576
45	2.040
35	1.920
2	1.817
25	1.660
20	1.592

*contamination from quartz

Order of Intensity	2θ	δ-spacing
w	26.35	3.382
w	28.60	3.121
w	32.15	2.784
1	42.85	2.110
vw	54.75	1.673
vw	61.15	1.516
vw	65.75	1.421

DATA FROM POWDER DIFFRACTION TABLES FOR BARITE

Intensity	δ-spacing
67	3.317
97	3.101
53	2.834
76	2.104
14	1.673
11	1.526
8	1.426

Tables 3.3, 3.4 and 3.5 Tables compare data obtained using the Gandolfi camera with values from experimental powder diffraction data for heulandite, analcime and rutile.

GANDOLFI CAMERA DATA

Order of Intensity	2θ	δ-spacing
w	17.20	5.150
w	18.95	4.685
1	22.60	3.930
2	30.20	2.960

DATA FROM POWDER DIFFRACTION TABLES FOR HEULANDITE

Intensity	δ-spacing
70	5.100
60	4.650
100	3.920
90	2.959

Order of intensity	2θ	δ-spacing
w	25.80	2.797
w	32.00	3.450

DATA FROM POWDER DIFFRACTION TABLES FOR ANALCIME

Intensity	δ-spacing
50	2.927
100	3.430

Order of intensity	2θ	δ-spacing
1	2.75	3.24
3	3.63	2.478
w	4.13	2.186
2	5.44	1.686
vw	5.63	1.634
vw	6.91	1.359

DATA FROM POWDER DIFFRACTION TABLES FOR RUTILE

Intensity	δ-spacing
100	3.25
50	2.487
25	2.188
60	1.6874
20	1.6237
20	1.3598

This hypothesis relies on minerals identified using x-ray diffraction. Evidence is far from conclusive though, since these minerals can form by means other than metasomatism.

One mineral that may have formed via metasomatic processes is barite. Barite was found in section F and as trace amounts in sections 4 and 5. This mineral has been documented to form terrestrially as a low temperature geochemical precipitate associated with low grade metamorphic and hydrothermal events. However, barite can form via other mechanisms as well, such as barium release during subaqueous volcanic activity (Church, 1979). If the latter is the case then the barite in these rocks is an original constituent.

Another mineral that may be the result of metasomatism is tourmaline (Plates 3.1 and 3.2). It is also a common associate of gold. In a study of 135 current and past producing 'gold-only' mines from the Superior province of the Canadian shield it was noted that tourmaline occurs in roughly two thirds of the deposits associated with quartz-bearing felsic volcanic rock (Hodgson, et al., 1980). The tourmaline, in these rocks, may be a metasomatic addition but unfortunately it can also form authigenically.

3.3 RETROGRADE METAMORPHISM

The effects of retrograde metamorphism were best represented by samples C, D and E. These samples are from the finely laminated felsic tuff, the second unit of the sampled

Plate 3.1 Photomicrograph of a tourmaline crystal oriented parallel to muscovite in section D. Cross nicols. Magnification is 63×.

Plate 3.2 Photomicrograph of same tourmaline crystal showing fractures perpendicular to foliation. Cross nicols. Magnification is 125×.


T

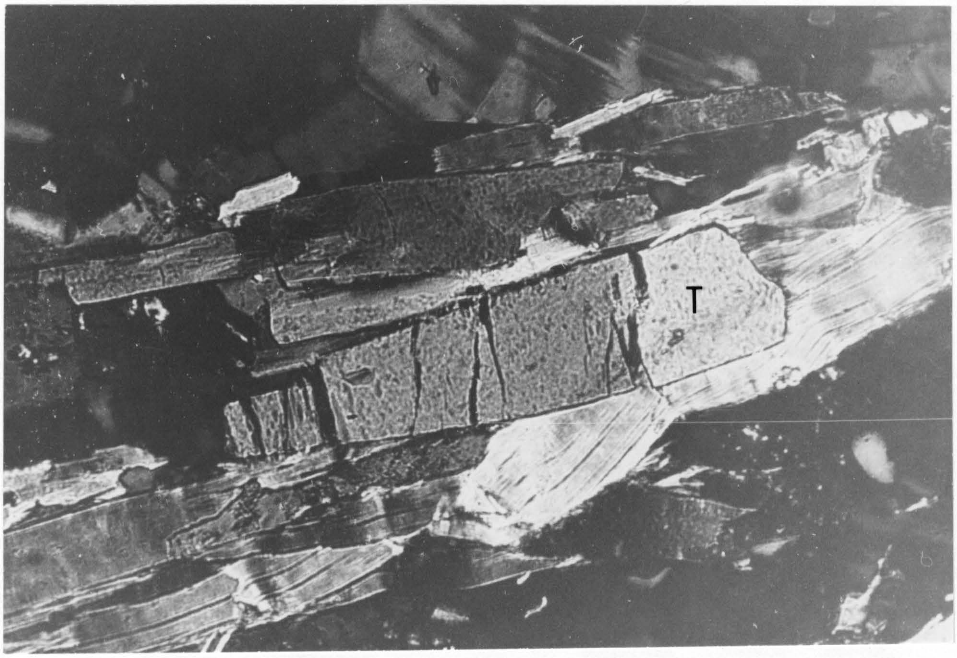
T

sequence. On the scale of a thin section alternating continuous bands of quartzo-feldspathic and micaceous material were noted.

In addition, also present were thicker discontinuous bands (Plates 3.3 and 3.4). The width of these bands was variable between 3.0 and 25 mm. To accentuate the discontinuous bands the rock slab was stained, by etching with 52 per cent HF (hydrofluoric acid) for approximately two minutes and then immersing it in saturated sodium cobaltinitrate solution for about one minute. The plagioclase shows up light grey, K-feldspar and muscovite are bright yellow and quartz is medium grey to glassy (Hutchinson, 1974).

A prominent constituent of the discontinuous bands was phenocrysts of plagioclase which were heavily altered to sericite (Plate 3.5). In section E one of the thicker bands was noted to contain the zeolites, heulandite and analcime as well (Plate 3.6). It is likely that the zeolites represent a retrograde assemblage since they are known to result from hydrothermal alteration. Zeolites most often occur as an alteration product of volcanic glass but calcic plagioclase is also an important precursor (Boles, 1977).

Corona texture was noted in the discontinuous bands of sections C and E. Anhedral grains of sphene in these slides were commonly surrounded by a rim of calcite.

Spherulites were also noted in section E (plate 3.7). They are present at the boundary between the continuous and the discontinuous bands. An attempt was made to identify the

Plate 3.3 Photograph of stained rock slab D distinguishing between yellow K-rich areas (muscovite + K-feldspar) and white plagioclase phenocryst regions. Magnification is 0.5×.

Plate 3.4 Photograph of same rock type, unstained, showing how the bands of plagioclase phenocrysts pinch out and are discontinuous. Magnification is 0.5×.

Plate 3.5 Photomicrograph showing plagioclase phenocryst (P) which has been heavily altered to sericite. Also note euhedral crystal of analcime (A) and porphyroblast of quartz (Q). Cross nicols. Magnification is 63×.

Plate 3.6 Photomicrograph showing the association of euhedral heulandite (H) with analcime (A). Cross nicols. Magnification is 63×.

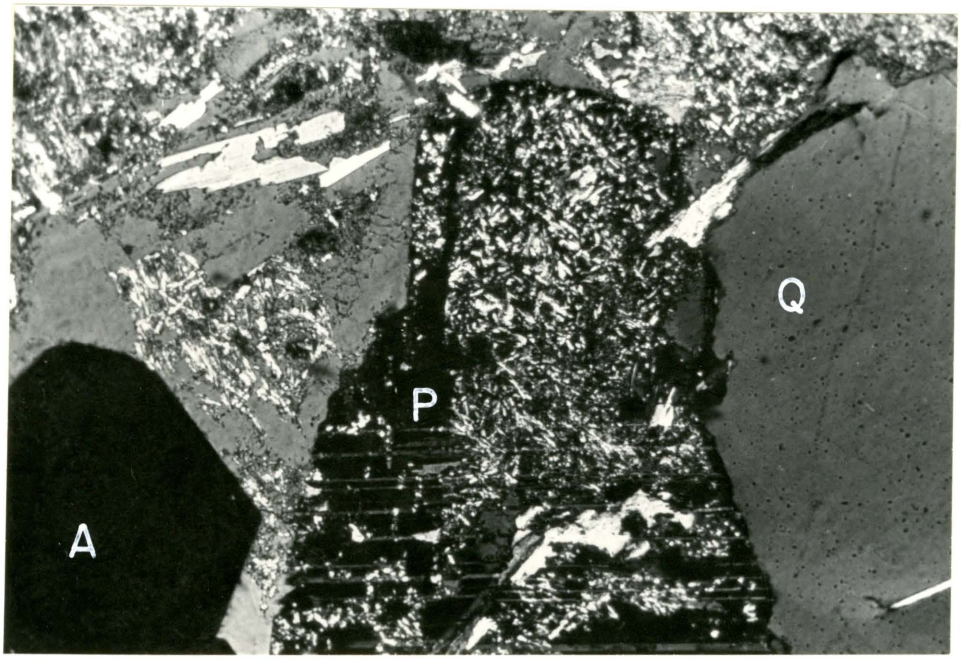
A
P
Q

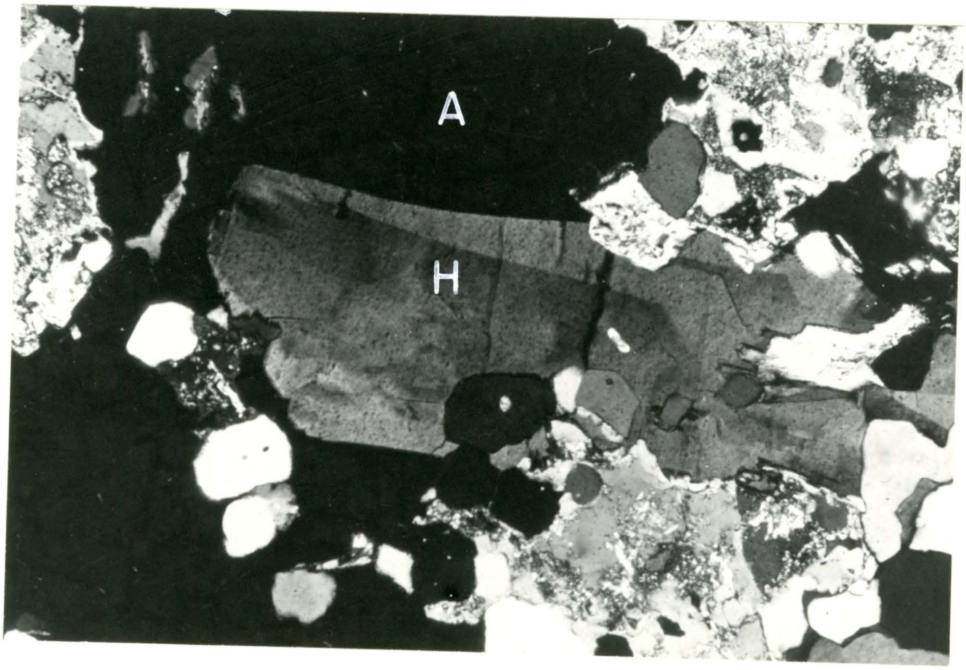
A
H

Plate 3.7 Photomicrograph showing spherulites which were present in section E. They occurred in small patches. Cross nicols. Magnification is 125×.

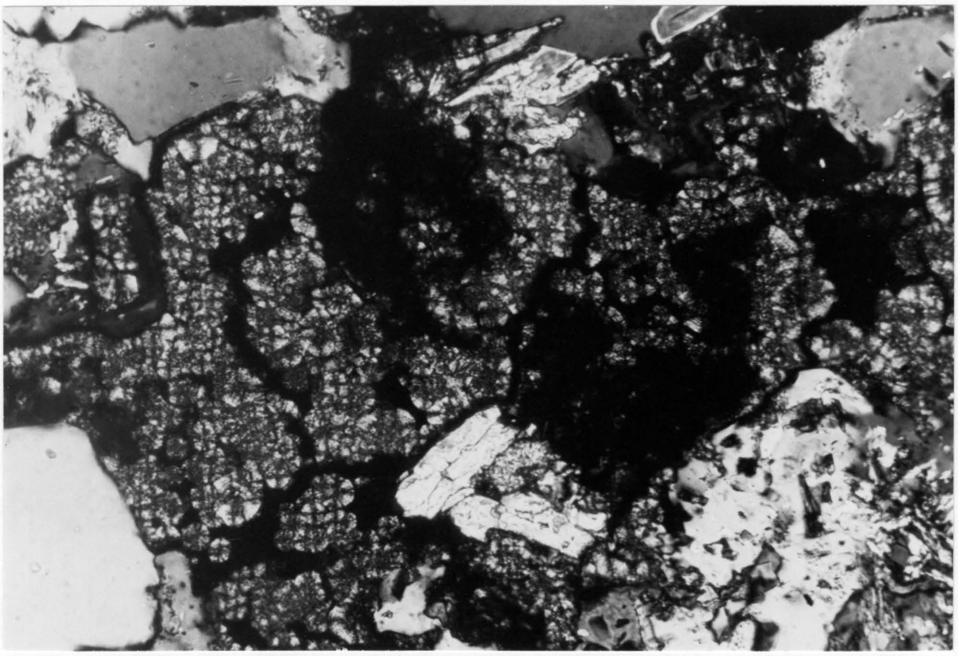

mineral making up the spherulites by using XRD but no pattern was obtained, indicating an amorphous structure.

All minerals and textures which have been interpreted as retrograde effects were contained within the discontinuous bands of sections C, D and E. It is likely that these discontinuous bands represent areas where fluids have seeped into the rocks, after metamorphism, parallel to the foliation.

CHAPTER 4

GEOCHEMISTRY

The analyses for the abundance of the ten major elements (Appendix 2) were acquired from X-Ray Assay Laboratories in Toronto. X-ray fluorescence (XRF) was used to obtain the values.

Errors for each individual oxide were also obtained from X-Ray Labs. A standard deviation was determined for each oxide by running 41 replicate analyses on each of two separate samples. The results are as follows:

	Sample 1	Sample 2
SiO_2	80.7±.25	65.9±.25
Al_2O_3	8.21±.06	13.0±.06
Fe_2O_3	4.87±.03	7.14±.03
K_2O	1.89±.01	2.51±.01
MgO	1.75±.02	6.08±.04
Na_2O	0.13±.01	0.60±.02
CaO	0.05±.005	0.72±.005

All numbers listed are in weight per cent.

The data was treated in two separate manners. First, it was used to classify the rocks and second, to determine if there were any specific trends in the oxides with respect to the concentration of Au in each sample.

4.1 CLASSIFICATION

4.1.1 ALKALIS VERSUS SILICA

This is a plot of total alkalis ($Na_2O + K_2O$) versus SiO_2, all in weight per cent (Fig. 4.1). It serves to differentiate between the subalkaline field (tholeiitic and calc-alkali series) and the alkaline field (alkaline and peralkine rocks). The dividing line on the graph was proposed by Irvine and Baragar (1971). The majority of samples lie in the subalkaline field so the entire assemblage was treated as such.

4.1.2 AFM DIAGRAM

The purpose of this ternary plot is to distinguish between the tholeiitic and the calc-alkali series (Fig. 4.2). Point A = $Na_2O + K_2O$; F = $FeO + .8998\ Fe_2O_3$; M = MgO (Irvine and Baragar, 1971). Values were calculated in weight per cent and then were normalized to 100 per cent to plot them. A value for FeO was obtained by applying the equation, $\%\ FeO = (\%\ Fe_2O_3 - \%\ TiO_2 - 1.5) \times 0.8998$. Since the samples plot below the dividing line (Irvine and Baragar, 1971) they make up a calc-alkaline suite. Calc-alkaline rocks tend to be richer in Al_2O_3 than tholeiitic ones.

Fig. 4.1 Plot of $(Na_2O + K_2O)$ versus SiO_2 in weight %. The majority of samples plot in the subalkine field.

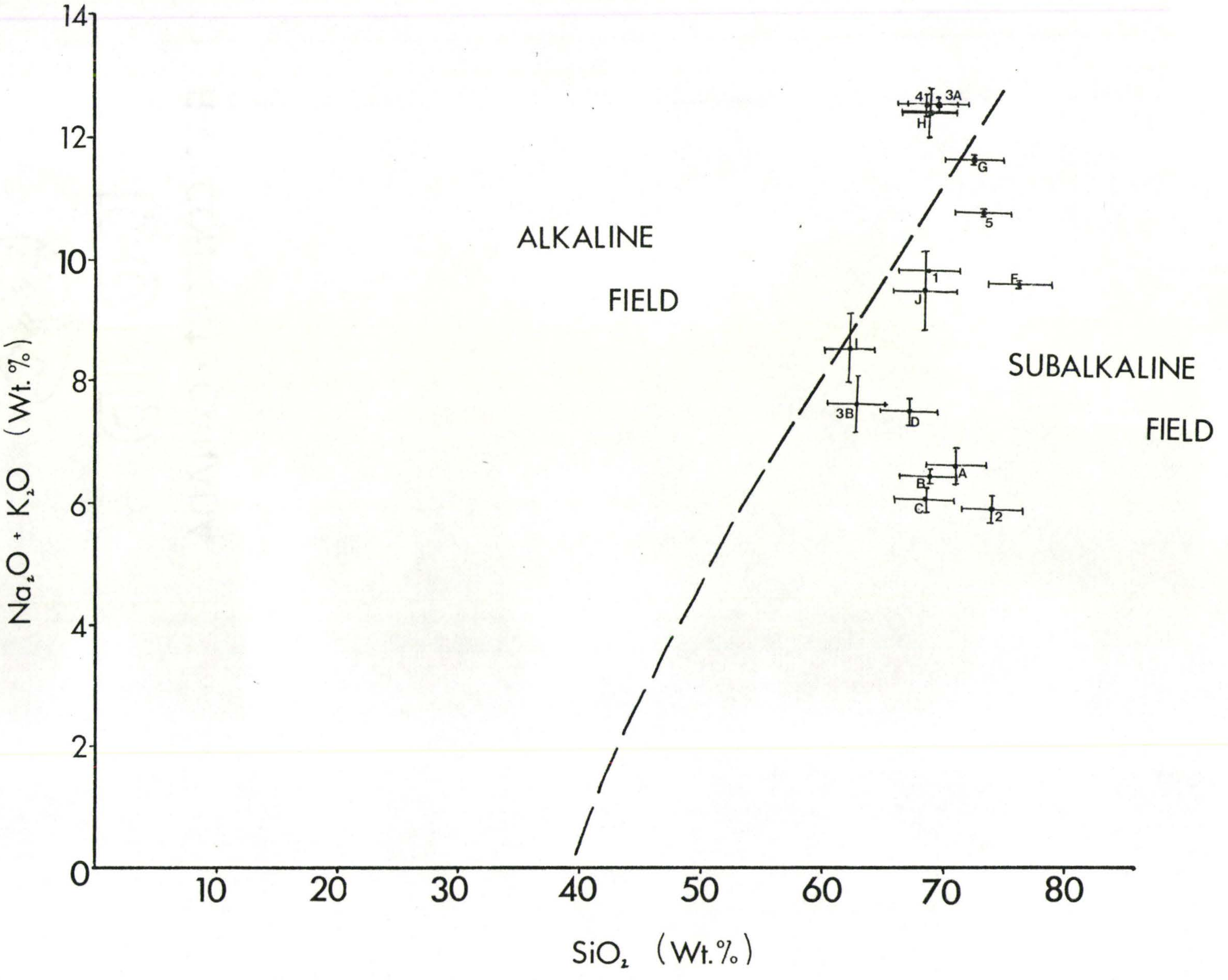

14
12
10
8
6
4
2
0
$Na_2O + K_2O$ (Wt. %)
10
20
30
40
50
60
70
80
SiO_2 (Wt. %)
ALKALINE
FIELD
SUBALKALINE
FIELD
4
3A
H
G
5
1
F
J
3B
D
A
B
C
2

Fig. 4.2 AFM diagram with A = Na_2O + K_2O; F = FeO + 0.8998 Fe_2O_3 and M = MgO. A calc-alkaline series is indicated.

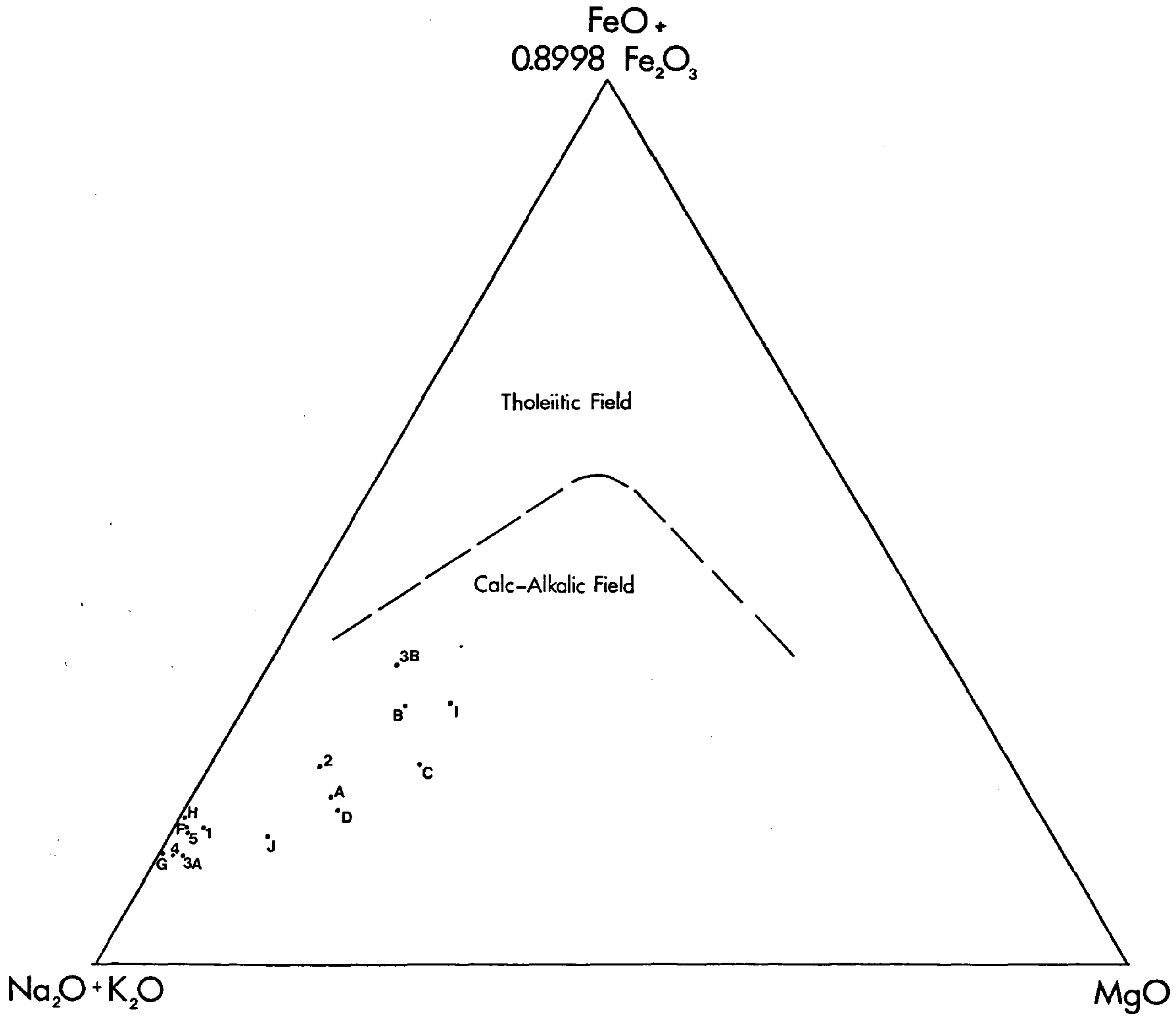
FeO +
0.8998 Fe_2O_3
Tholeiitic Field
Calc–Alkalic Field
3B
B
I
2
C
A
D
H
P
5
1
J
4
G
3A
$Na_2O + K_2O$
MgO

4.1.3 JENSEN CATION PLOT

This ternary plot (Jensen, 1976) was used to further subdivide the calc-alkaline series and to apply suitable rock names (Fig. 4.3). The three apices are Al_2O_3; MgO; $FeO + Fe_2O_3 + TiO_2$, all in mole per cent (normalized to 100%). FeO was calculated as in the previous plot.

The Jensen plot agrees with the AFM diagrams in that the majority of samples are in the calc-alkaline field, although one sample (sample H) plots in the tholeiitic field. Almost half the samples (F, G, H, 1, 3A, 4, 5) have the composition of a rhyolite, four samples (A, D, J, 2) plot in the andesite field and one (I) has the composition of basalt.

In greenstone belts there is generally an increase in calc-alkaline components with stratigraphic height (Goodwin, 1977). These rocks appear to represent the final stages in the evolution of a volcanic pile. The majority of the samples have the composition of a rhyolite and the only sample to have the composition of a basalt is a sill.

4.2 VARIATION OF OXIDES WITH RESPECT TO GOLD

Before any of these diagrams could be plotted the amount of Au had to be determined for each sample. This was done by using Instrumental Neutron Activation Analysis (INAA). Nine samples were run along with two chemical standards.

Fig. 4.3 Jensen cation plot. This was used to give names to individual samples.

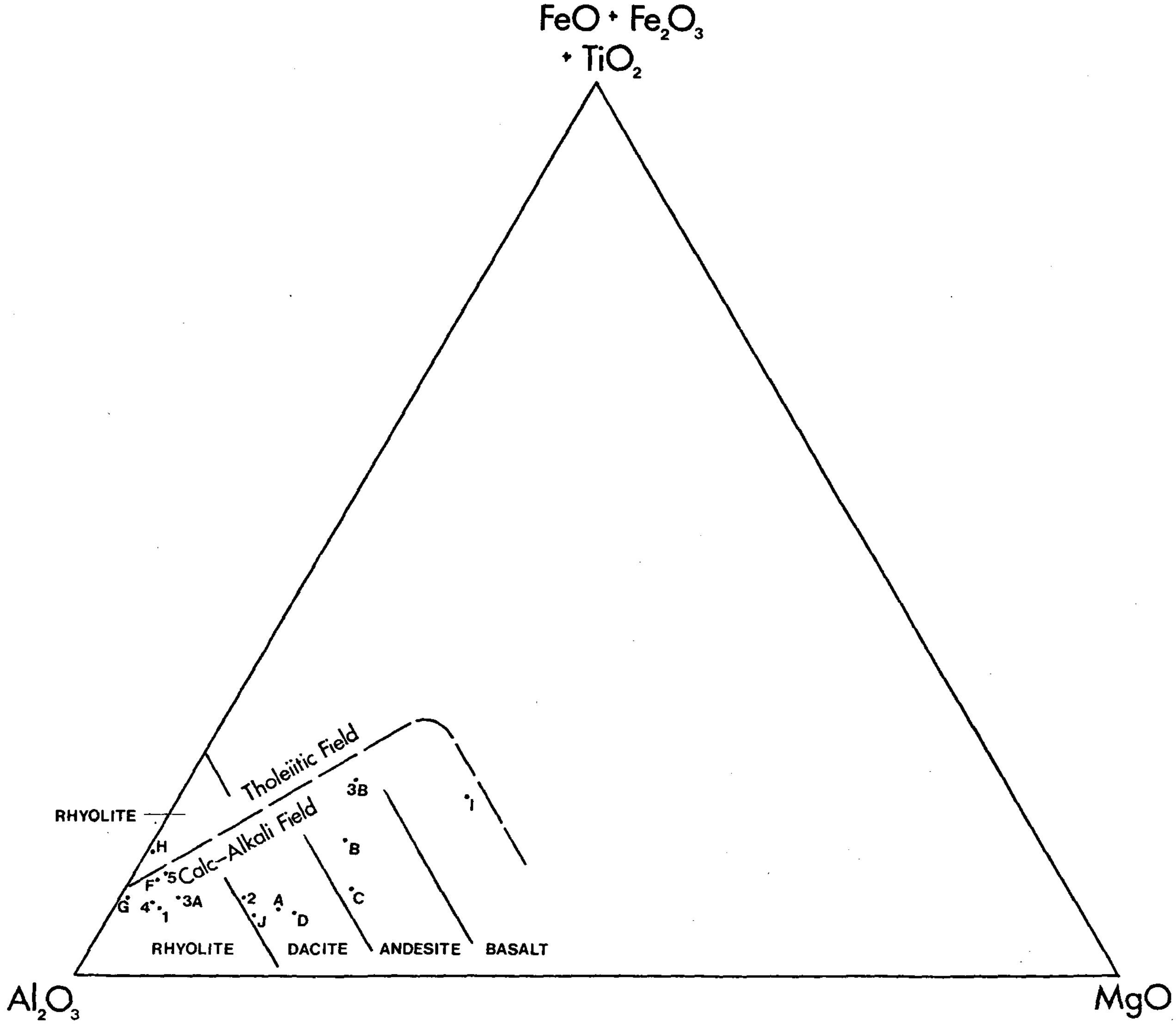
FeO + Fe_2O_3 + TiO_2
Al_2O_3
MgO
Tholeiitic Field
Calc-Alkali Field
RHYOLITE
RHYOLITE
DACITE
ANDESITE
BASALT
H
F
5
G
4
1
3A
2
J
A
D
C
B
3B
I

4.2.1 METHOD OF ANALYSIS

This is a standard inhouse process used at McMaster University. The procedure remains unpublished.

First the rocks were broken up into small chips by putting each sample through a pulverizer. These chips were in turn placed inside a tungsten-carbide grinding dish which was then strapped on to a shatterbox for further size degradation.

Approximately 500 mg of each powdered sample was weighed. The chemical standards were prepared by doping acid-washed quartz powder with a known concentration of Au in solution, and they were then allowed to dry slowly. Each sample and chemical standard was contained in its own plastic vial.

Once the standards were dry, the nine samples and two standards were bundled together and irradiated in the McMaster reactor for 1.0 MwH in a cadmium shielded, high flux facility (flux density = 1.5×10^{13} neutrons/cm^2/sec). The cadmium shield was used to enhance Au irradiation and suppress irradiation of other elements, especially Na. In the reactor ^{197}Au undergoes the reaction $^{197}Au(n,\gamma)^{198}Au$.

After a four day cooling period the samples were counted for one-half hour each. The 0.412 MeV photo peak was counted since this corresponds to ^{198}Au. Au counts were corrected for decay (Table 4.1) during the count period by applying the formula; $A = A_o e^{\lambda t}$ where:

A = corrected counts

A_0 = original count

λ = decay constant = $\frac{.693147}{^{198}\text{Au half-life}}$

^{198}Au half life = 64.704 hrs.

t = time elapsed after first count.

To convert these counts to parts per billion (PPB) each sample had to be compared to the two standards. For each standard the corrected count was divided by the amount of gold per gram in that standard (Table 4.1) and an average of these two numbers was taken.

To get the weight of Au, in each sample, the corrected counts were divided by the average number obtained from the standards. To convert this number to PPB it was divided by the weight of the sample and multiplied by 1000.

4.2.2 ABUNDANCE OF GOLD

In a study on the background content of gold in major rock types (Crockett, 1978) it was noted that in both plutonic and volcanic rocks the gold content decreases from mafic to felsic types. In another study the average gold content of gabbros and basalts was determined to be about 7 PPB, for diorites and andesites 5 PPB and for granites and rhyolites 3 PPB (Boyle, 1982).

Table 4.1 Table shows calculations carried out to determine the abundance of gold in nine samples tested.

ABUNDANCE OF Au (PPB) FROM NEUTRON ACTIVATION ANALYSIS

Sample	Original Count (A_0)	Time (hrs)	Corrected Count (A)	Weight of Au per gram (μgm)	$\frac{\text{Corrected Count}}{\text{Weight of Au per gram}}$ (μgm^{-1})
STND 1	7619	9.33	8420	.18049	45888
STND 2	8202	-	8202	.18290	44844
				mean =	45366

Sample	Original count (A_0)	Time (hrs)	Corrected Count (A)	Weight of sample (gm)	Weight of Au in sample (μgm)	Au (PPB)
C	2001	1.33	2029.8	.50565	.0447426	88.49
D	1039.5	1.95	1061.4	.50085	.0233963	46.71
D_s	1622	2.60	1667.8	.50638	.0367631	72.60
G	9537	3.48	9899.6	.49835	.2182157	437.88
F	11482	4.45	12042.7	.51716	.2654558	513.30
A	1666	5.12	1759.9	.49484	.0387933	78.40
H	3520	5.92	3750.3	.51853	.0826674	159.43
J	779	7.07	840.2	.47848	.0185204	38.71
2	1634	8.37	1787.2	.51776	.0393950	76.09

It is evident that all samples analysed in this study have values above background gold (Table 4.1). Sample F, which has the composition of a rhyolite has concentrations of gold almost 200 times that of an average rhyolite.

Analytical precision for samples having approximately 100 PPB gold is estimated to be ±20% based on the replicate analysis of an in-house standard (B4-2268; Fyon, personal communication, 1983).

4.2.3 VARIATION RESULTS

The analysis of seven major oxides (Al_2O_3, CaO, Fe_2O_3, K_2O, MgO, Na_2O and SiO_2), all in weight per cent were plotted against the concentration of gold, in PPB.

For sample D two separate zones were analysed. One was the well banded zone containing alternating but continuous layers (designated vial D) and the other was the sericitized plagioclase phenocryst zone (designated vial D_s). This was done to determine whether gold was more concentrated in one zone than the other. As it turned out the gold was a little higher in the sericitized plagioclase zone but not by a significant factor. To plot sample D on the variation diagrams the average gold concentration between the two samples (D and D_s) was used.

The samples with the highest concentrations of gold (F and G) are associated with high concentrations of SiO_2 (Fig. 4.4) and K_2O (Fig. 4.5) and low concentrations of Al_2O_3 (Fig. 4.6), MgO (Fig. 4.7), Na_2O (Fig. 4.8), CaO (Fig. 4.9) and total Fe as Fe_2O_3 (Fig. 4.10).

Fig. 4.4 Graph of SiO_2 (wt. %) versus Gold (PPB).

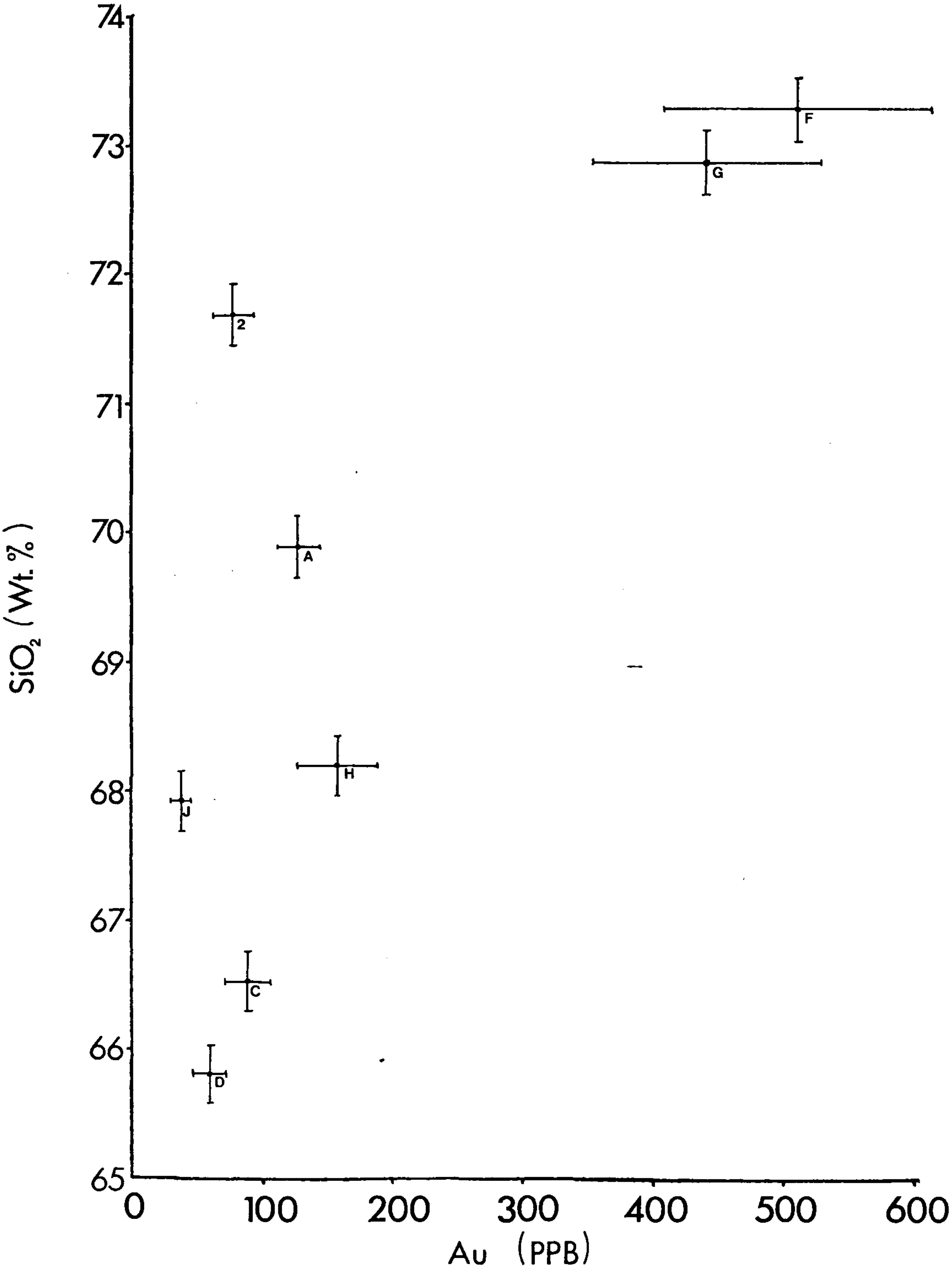
74
73
72
71
70
69
68
67
66
65
SiO2 (Wt. %)
F
G
2
A
H
J
C
D
0
100
200
300
400
500
600
Au (PPB)

Fig. 4.5 Graph of K_2O (wt. %) versus Gold (PPB).

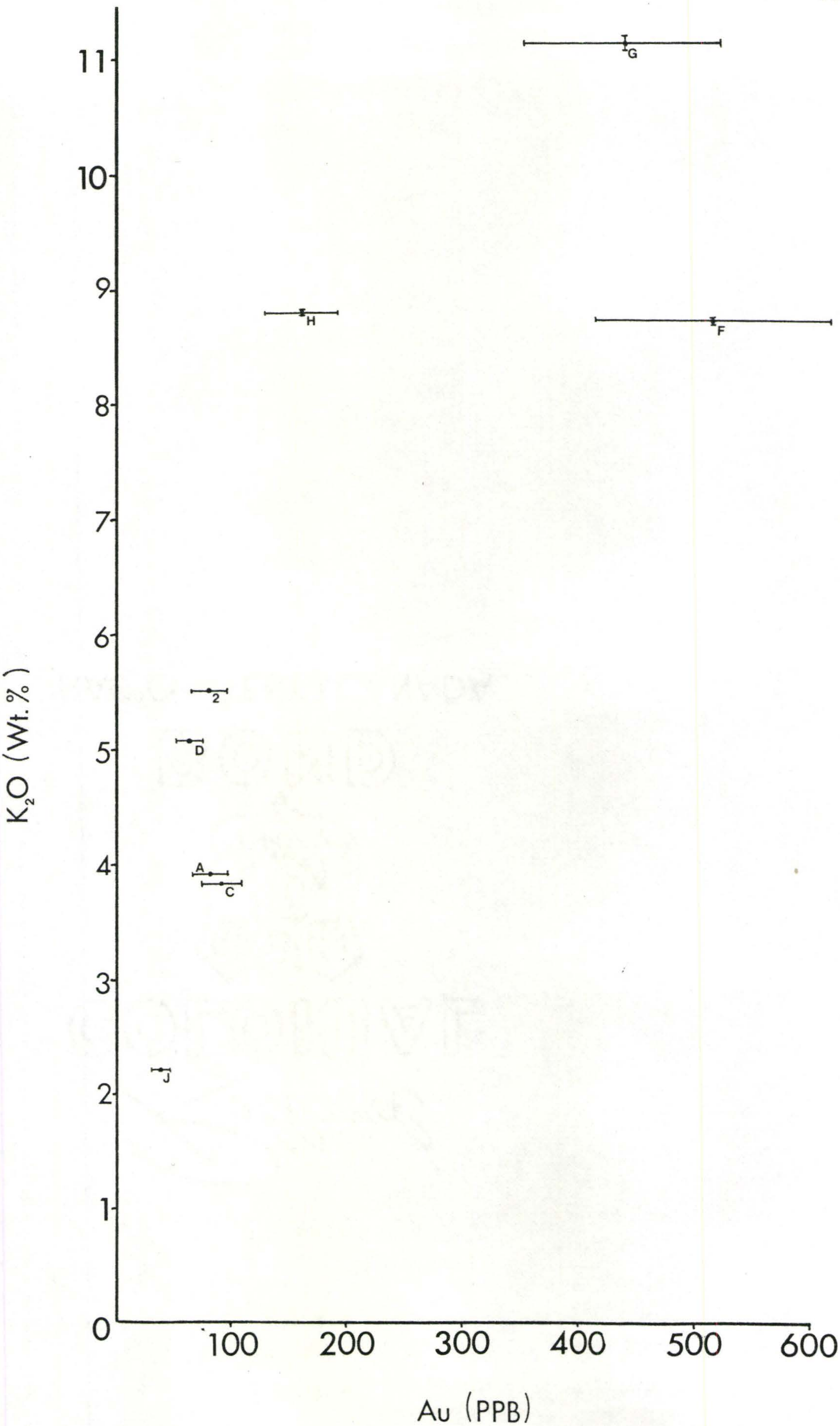

11
10
9
8
7
6
5
4
3
2
1
0
100
200
300
400
500
600
K2O (Wt.%)
Au (PPB)
G
H
F
2
D
A
C
J

Fig. 4.6 Graph of Al_2O_3 (wt. %) versus Gold (PPB).

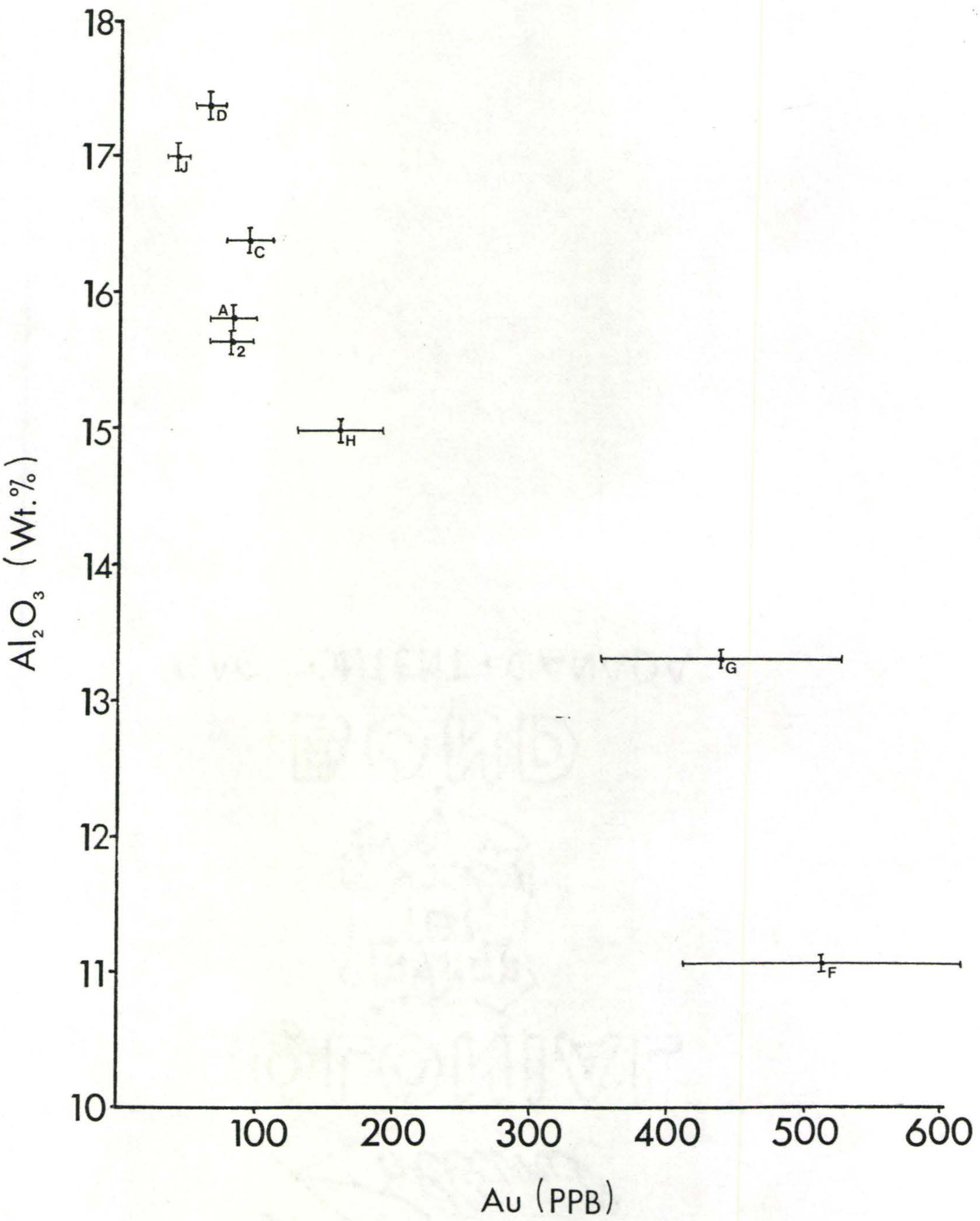
18
17
16
15
14
13
12
11
10
100
200
300
400
500
600
Al_2O_3 (Wt.%)
Au (PPB)
D
J
C
A
2
H
G
F

Fig. 4.7 Graph of MgO (wt. %) versus Gold (PPB).

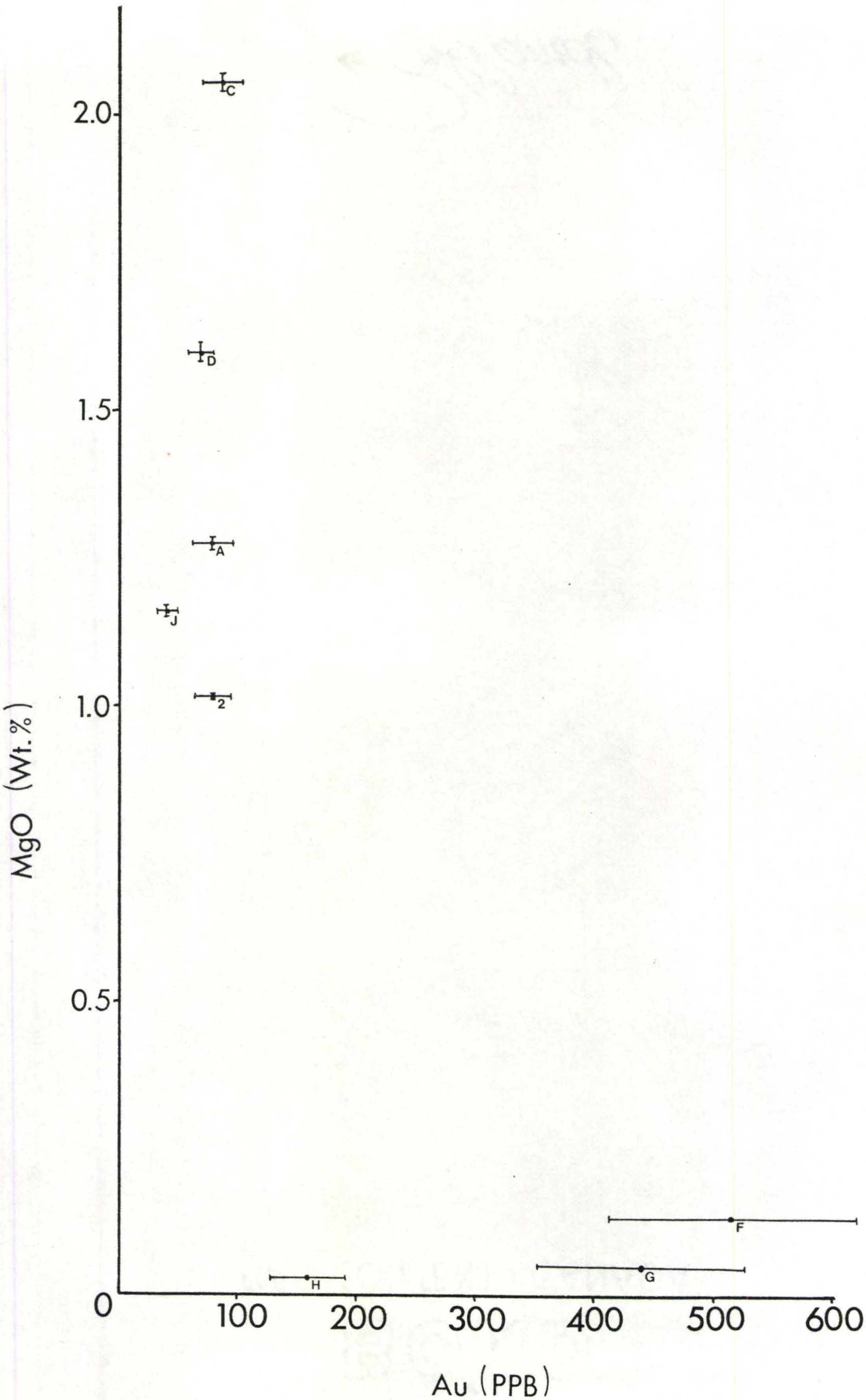

MgO (Wt.%)
2.0
1.5
1.0
0.5
0
C
D
A
J
2
F
G
H
100
200
300
400
500
600
Au (PPB)

Fig. 4.8 Graph of Na_2O (wt. %) versus Gold (PPB).

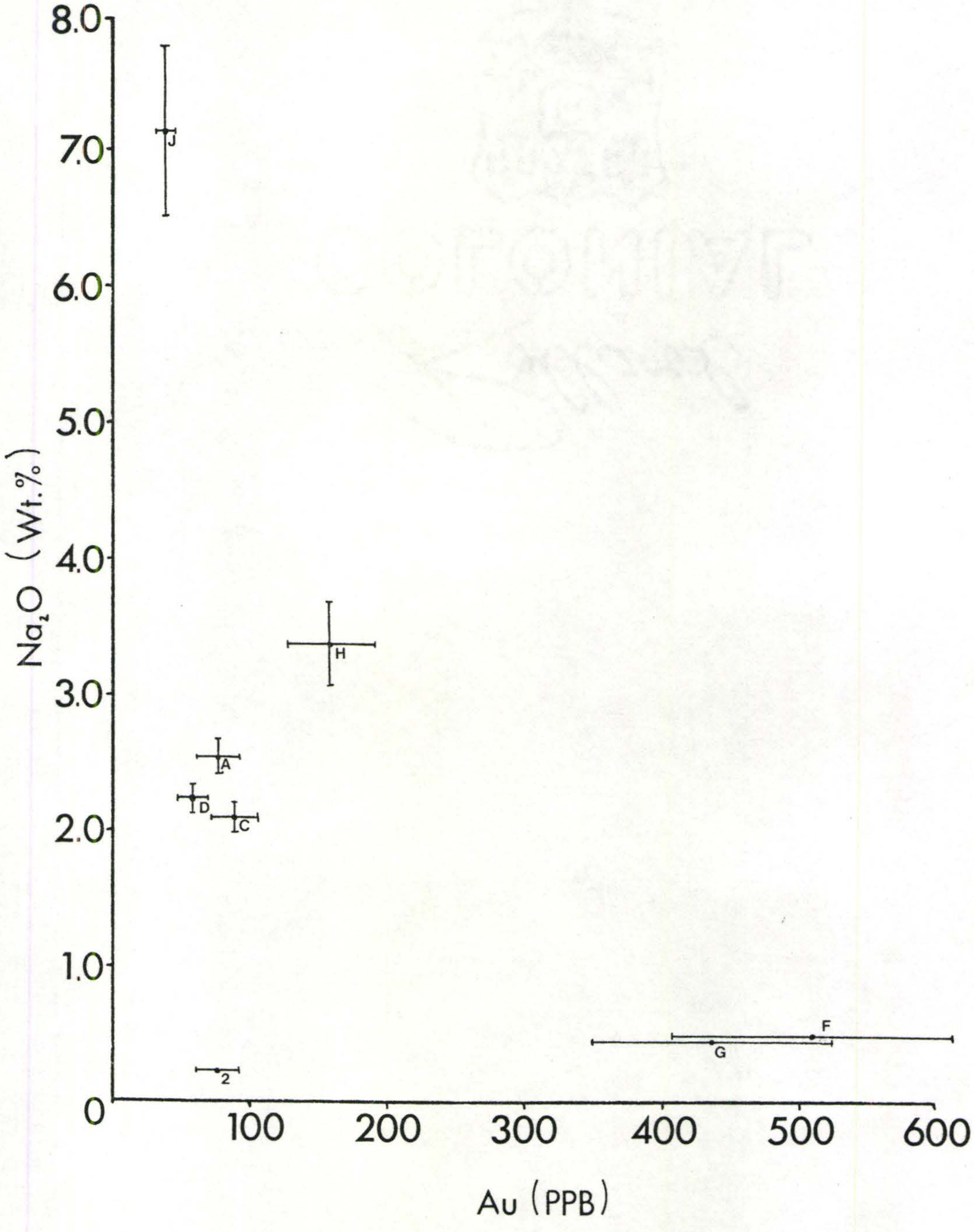
8.0
7.0
6.0
5.0
4.0
3.0
2.0
1.0
0
Na_2O (Wt.%)
J
H
A
D
C
2
F
G
100
200
300
400
500
600
Au (PPB)

Fig. 4.9 Graph of CaO (wt. %) versus Gold (PPB).

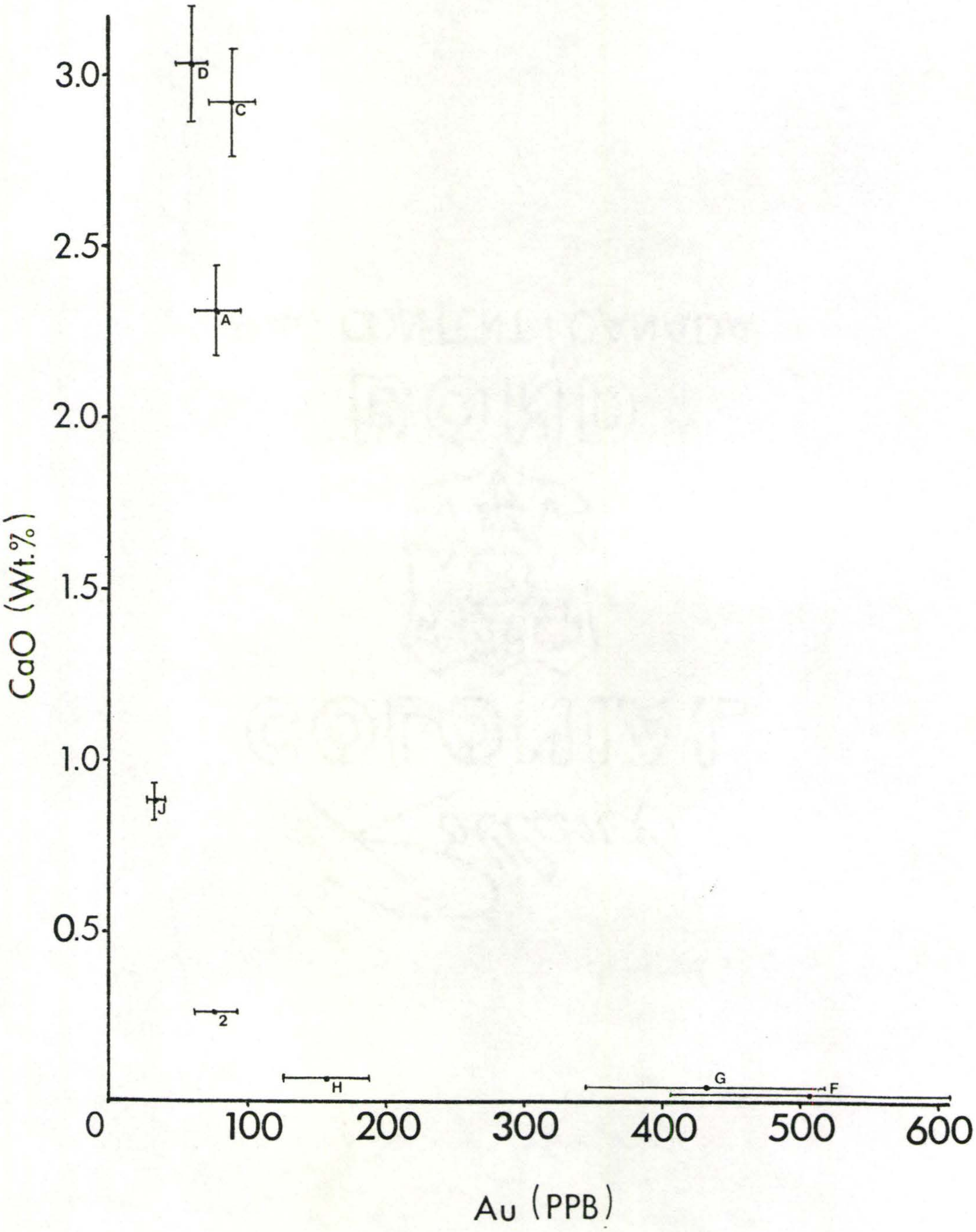

CaO (Wt.%)
3.0
2.5
2.0
1.5
1.0
0.5
0
100
200
300
400
500
600
Au (PPB)
D
C
A
J
2
H
G
F

Fig. 4.10 Graph of Fe_2O_3 (wt. %) versus Gold (PPB).

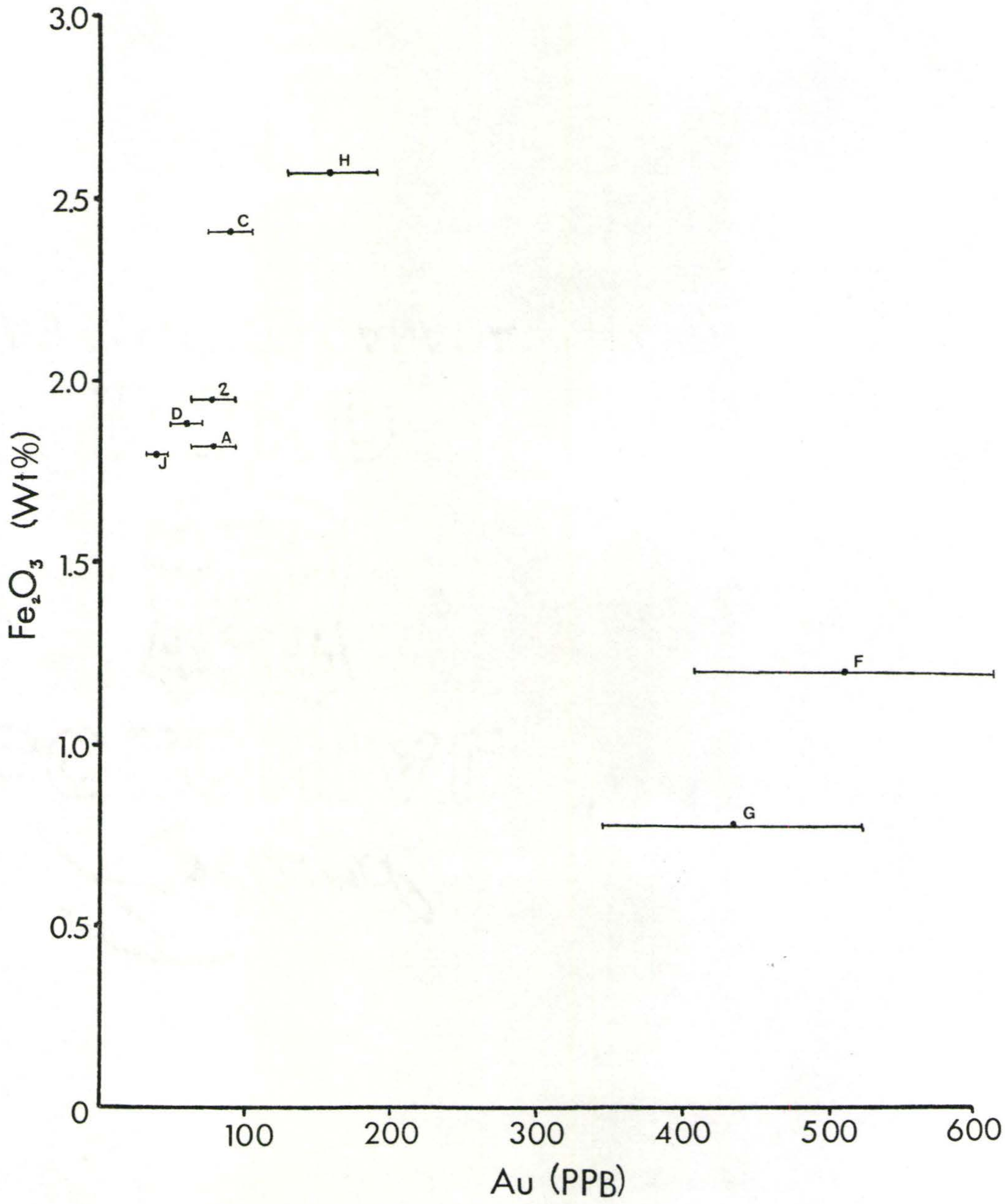
3.0
2.5
2.0
1.5
1.0
0.5
0
Fe_2O_3 (Wt%)
H
C
2
D
A
J
F
G
100
200
300
400
500
600
Au (PPB)

Table 4.2 Estimated mineral abundances for each thin section.

Mineral / Section	Quartz: Groundmass	Quartz: Porphyroblasts	K-Spar	Plaglioclase: Groundmass	Plaglioclase: Phenocrysts	Musc.	Bio.	Chlorite	Tour.	Bar.	Sphene	Cc.	Rutile	Heu.	Analc.	Garnet	Zir.	Epidote	Opaque
C	30	10	10	9	3	30			1		tr.	tr.	tr.			tr.			4
D	22	8	20	13	2	30			1			tr.	tr.			tr.			2
G	11	14	70			tr.					tr.								4
F	54	3	30	2		1	2			3	tr.		tr.						4
A	30	10	10	13	1	19	11	tr.	tr.		tr.	tr.	tr.			tr.			3
B	35		16	10		20	12	3				1	1			tr.			2
E	24	10	3	11	4	30	3		tr.		1	tr.	1	3	7				2
H	17	13	50	1	15	tr.					tr.								3
I	20		10	35		5	25	tr.				4					tr.		
J	9	15	24	15	15	10		10			tr.	1				tr.			1
1	23	12	30			34													1
2	48	6	2			40		tr.	1			1				tr.			1
3A	14	2	70	2		tr.	5	3				2							2
3B	10		25			15	20	3			tr.	5					tr.	6	1
4	38	5	37	3		8	4	tr.	tr.	tr.		1					tr.		3
5	15	15	59	1		1	2	3		tr.	tr.	tr.				tr.			3

The high and low concentrations of the oxides parallel the mineralogy seen in the thin sections (Table 4.2). The high K_2O values are associated with a high percentage of microcline while high SiO_2 is associated with quartz and microline.

The low Na_2O and CaO values are probably due to a lack of plagioclase in the high gold samples. The low Al_2O_3 can be explained by a deficiency in muscovite.

Low concentrations of MgO and Fe_2O_3 in the high gold samples infers that the gold is in no way tied to the mafic component of these rocks. A lack of tourmaline (dravite) and/or chlorite accounts for the low MgO. The low Fe_2O_3 is related to low biotite and lack of chlorite and possibly ilmenite. The low Fe_2O_3 is not related to the pyrite content since the gold-rich samples appear to have substantial pyrite in hand specimen.

Since the samples are only from the footwall of the Hemlo ore zone these trends are difficult to compare with trends cited for other ore bodies. However if it is assumed that the amount of gold correlates with the amount of alteration, then one comparison can be made.

In the Bousquet, Quebec deposit, gold occurs in a number of stratiform pyritic lenses. A mafic tuff lies directly below the ore zone in one lens that was studied. As this lens was approached from the footwall an increase in K_2O and SiO_2 along with a decrease in MgO, Na_2O and CaO was noted (Valliant, et al., 1980b). This deposit has been interpreted as syngenetic by these authors.

These results are similar to the ones obtained for the the footwall of the Hemlo ore body. Trends for Al_2O_3 in the Bousquet deposit were not reported.

CHAPTER 5

GOLD IN THE HEMLO AREA

It has been postulated that the gold ore body at Hemlo may be syngenetic (Valliant, 1982). The term implies that the gold was an original constituent of the rocks and that it was not introduced by ore-forming fluids during some later event. This is an attempt to look at some common characteristics of gold orebodies that may be syngenetic and to see if any of these characteristics apply to Hemlo.

5.1 GREENSTONE BELTS

As mentioned in the introduction, the Hemlo area is part of a small greenstone belt. Since there seems to be a common association between greenstone belts and the occurrence of major gold bodies an explanation of this term is in order.

The term refers to bands of metamorphosed volcanic rocks and associated sediments which occur in the Archean shield regions of the world. The word greenstone alone relates to the mineralogy of the altered basic igneous rocks which often consist of different proportions of chlorite, hornblende and epidote.

Each volcanic pile within a greenstone belt displays a general compositional progression from dominantly tholeiitic basalt in lower parts of the sequence to dacite and locally rhyolite at the top. The ratio of basalt:andesite:dacite: rhyolite is approximately 50:30:10:5 (Goodwin, 1977).

The Hemlo deposit is associated with felsic volcanic rocks and overlying sediments. Therefore it occurs at the top of a volcanic pile.

By analogy with modern environments a more or less oceanic setting is implied for the greenstone belts, however associated andesites and rhyolites suggest at least local evolution of island arc conditions. Therefore, the greenstone belts may represent remnants of oceans and volcanic arcs formed between incipient continents. The remains of these continents may be the gneissic regions of the shields that we see today (Dott and Batten, 1981).

5.2 POSSIBLE SYNGENETIC GOLD

Three separate ore zones of possible syngenetic origin were compared. All of these deposits are located on the Abitibi greenstone belt which is further east than the Marathon-Schreiber belt of which Hemlo is a part. The deposits looked at were: Agnico-Eagle, Quebec, (Barnett, et al., 1982); Bousquet Region, Quebec, (Valliant, et al., 1982 a,b); Ankerite units, Dome Mine, Timmins, (Fryer et al., 1979; Karvinen, 1980).

The first criteria looked at was the relation of the ore to stratigraphy. The ore of the Agnico-Eagle deposit and the Dome ankerite units are stratibound. The ore of the Bousquet deposit is described as being stratiform since it is confined to conformable pyritic lenses which lie directly on top of the footwall rocks.

Next, associated lithologies were considered. Stratiform gold ores of possible syngenetic origin appear to be confined to deposits in which felsic volcanic rocks are present (Hodgson, et al., 1980). This is stratigraphically near the top of a volcanic pile in a greenstone belt. Felsic tuffaceous rocks are associated with the ore zones of all three locations.

Gold is present in these deposits as the native metal as well as minor tellurides in two of the deposits. The gold is usually associated with a sulfide such as pyrite. Associated minerals in the three deposits are variable. Pyrite and pyrrhotite are associated at Agnico-Eagle while pyrite and chalcopyrite are associates at Bousquet. The ankerite unit at Dome has a number of associated minerals including tourmaline, scheelite and fuchsite, a chromium-rich mica.

The final criteria looked at were size and grade. The ore at Agnico-Eagle and Bousquet is of large tonnage and low grade while the ore of the Dome ankerite unit is of small tonnage and high grade.

The authors of these papers envisage the same basic model for syngenetic gold, one of exhalative chemical sediments associated with explosive felsic volcanism. To complete this model a source is needed for the explosive pyroclastics. For the Bousquet region a proposed source is a small granodiorite stock which may represent an ancient magma chamber. In the Dome mine area a brecciated zone has been noted which is interpreted as a vent for the exhalites and the felsic volcanism.

5.3 HEMLO GOLD

The following description of the Williams ore body was obtained from Bob Valliant (personal communication, 1983).

The ore body on the Williams property occurs at the junction between the felsic tuffaceous rocks, which are the object of this study, and the overlying pelitic metasedimentary rocks. The ore is stratabound but in many places appears to be stratiform.

The majority of the gold occurs as the native metal within silicate groundmass but a minority of it is associated with pyrite. Common accessory minerals are molybdenite and stibnite.

It has recently been inferred that four million tons of ore are present, grading at 0.16 ounces per ton. This is large tonnage and low grade ore.

The Hemlo ore body seems to compare most favourably with the Bousquet deposit. The Dome ankerite unit is not of the same scale and the Agnico deposit is based on a facies relationship which is not present at Hemlo. One difference between the Hemlo and the Bousquet deposits is in the associated minerals. Molybdenite is an associate of the Hemlo gold. This is no problem since associated minerals commonly vary from deposit to deposit anyway.

No lithology nor structure has yet been mapped which could be interpreted as a source for exhalative ore-bearing fluids and felsic pyroclastics at Hemlo. However it is very possible than an ancient source exists under Moose Lake (Fig. 1.1).

Sample 5 is a piece of core from a unit that lies directly below Moose Lake. It is distinctly granitic looking rock with a strong foliation indicating that it has undergone the same metamorphism that the tuffs have undergone. The mineralogy of this rock is very similar to that of the tuffs (Table 4.1).

It is possible that this rock is part of a small granitic pluton that represents an ancient magma chamber. This magma chamber could have been the source for the gold and the felsic pyroclastics found at Hemlo.

CHAPTER 6

CONCLUSION

There are two possible origins for the gold at Hemlo. One is a syngenetic origin where the gold would have been introduced during the emplacement of the tuffs and the other is an epigenetic origin where the gold would have been introduced after the emplacement of the tuffs.

It has been determined that these tuffaceous rocks have undergone extensive metamorphism. Metamorphic textures such as polygonalized grain boundaries within the groundmass, sutured grain boundaries within porphyroblasts of quartz and the preferred orientation of platey minerals are abundant. Retrograde metamorphic effects such as the introduction of zeolites and a reaction rim around sphene appear to be confined to the discontinuous bands in samples C, D and E. The gold concentration is slightly higher in these zones when compared to the zones in the same samples which show no retrograde effects, however, this is not by a significant amount.

Minerals such as barite and tourmaline suggest that these tuffs have been exposed to metasomatic fluids. It is possible that the gold was introduced with these metasomatic fluids during metamorphism. This method favours an epigenetic origin for the Hemlo gold.

On the other hand these metamorphic effects may have taken place after the introduction of the gold. The samples of this study appear to represent the felsic phases of a volcanic pile which, in greenstone belts, is near the stratigraphic top. The ore itself is present at the top of this felsic pile. This is unusual since most gold camps are located at or near the top of a mafic-ultramafic sequence (Hodgson and MacGeehan, 1980).

Gold concentrations are well above background gold in all samples tested including sample J which is a felsic sill. The gold is associated with high weight per cents of SiO_2 and K_2O and low weight per cents of Al_2O_3, CaO, Fe_2O_3, MgO and Na_2O. The low Fe_2O_3 and MgO shows how the gold is in no way associated with the mafic components of these tuffs.

The Hemlo gold deposit is stratibound and in many places appears stratiform. It is associated with explosive felsic volcanics and a felsic pluton of similar mineralogy is nearby which may represent the ancient magma chamber for the felsic pyroclastics and the ore-bearing fluid. This felsic pluton has been metamorphosed to the same degree as the tuffs indicating that it was present before the metamorphic event.

In these and other respects the Hemlo gold is very similar to the deposit at Bousquet, Quebec which has been interpreted as a syngenetic deposit (Valliant, et al., 1980 a,b). therefore it is very possible that the ore at Hemlo is of syngenetic origin.

This study is not conclusive in proving whether the Hemlo ore is of epigenetic or syngenetic origin. The rocks sampled were taken only from the footwall. Furthermore only a limited number of samples were dealt with and more extensive work would have to be done before any conclusion could be made.

Further work would entail correlating the data obtained from this study on the footwall rocks with data from rocks of the ore zone. The metamorphism and metasomatism should also be studied more extensively to determine if the gold is associated with these events. Addition and depletion trends of the oxides versus the concentration of gold should also be looked at closer to see if they are real trends or if they only represent different lithologies.

Errors in this study include estimated model abundances of the thin sections. Better estimates could have been obtained using a point count method. There was also error involved in the whole rock analysis using XRF and in determining the concentration of gold using neutron activation but these errors were taken into account.

APPENDIX 1

THIN SECTION ANALYSIS AND SKETCHES

SECTION A:

MINERALOGY:		MODAL ABUNDANCE (%)
1)	Quartz	40
2)	Plagioclase	14
3)	Microcline	10
4)	Muscovite	19
5)	Biotite	11
6)	Chlorite	tr.
7)	Tourmaline	tr.
8)	Sphene	tr.
9)	Rutile	tr.
10)	Calcite	tr.
11)	Garnet	tr.
12)	Opaque	3

This section shows a distinct lepidoblastic texture due to the parallel alignment of micas. Most of the mica has euhedral crystal shape with sharp boundaries but some grains were not as well defined and had mottled extinction. The average length was 0.20 mm.

Polygonal crystallization was common among the quartzo-feldspathic material. All quartz and feldspar grains are anhedral with an average grain size of 0.10 mm.

Porphyroblasts of quartz are an abundant constituent. They were elongated parallel to the alignment of the mica and reached up to 3.0 mm in size. Most of the porphyroblasts had subgrains with weakly sutured boundaries and inclusions of both biotite and muscovite. All quartz in this section showed strained extinction.

Phenocrysts of plagioclase, up to 1.0 mm in size, were also identified. They were patchy looking due to alteration to both sericite and calcite.

Tourmaline was the most abundant of the accessory minerals occurring as tiny subhedral grains, parallel to the mica. Sphene occurred as anhedral crystals reaching 0.04 mm in size and was commonly surrounded by a rim of calcite. Minor amounts of rutile were noted in the slide, always together with an opaque. Garnet took the form of very tiny euhedral crystals up to 0.02 mm.

Subhedral to euhedral opaques, that were not associated with rutile, were disseminated throughout the slide. Size of the grains varied from 0.01 to 1.20 mm.

THIN SECTION A

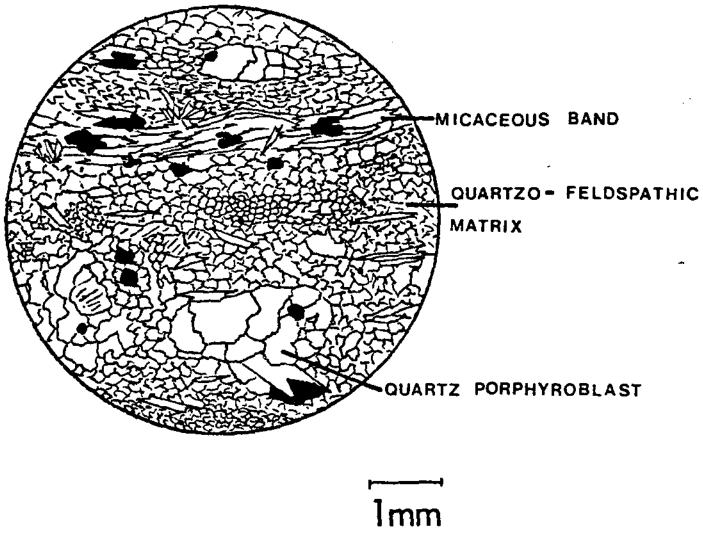

SECTION B:

MINERALOGY:

		MODEL ABUNDANCE (%)
1)	Quartz	35
2)	Orthoclase	16
3)	Plagioclase (labradorite An_{59})	10
4)	Muscovite	20
5)	Biotite	12
6)	Chlorite	3
7)	Rutile	1
8)	Calcite	1
9)	Garnet	tr.
10)	Opaque	2

This section has a weak foliation due to the subparallel alignment of biotite and chlorite. The biotite ranges from single euhedral crystals as small as 0.02 mm to aggregates of crystals up to 1.0 mm in length. Chlorite ranges from tiny crystals of 0.05 mm to felted aggregates of crystals as large as 1.5 mm.

Muscovite is present as large poikiloblasts, up to 3.0 mm in length, with no preferred grain orientation. Inclusions of quartz were common in the poikiloblasts.

Polygonal crystallization was noted in the quartzo-feldspathic material in the slide but this was not always distinct. Grain size was variable from 0.02 to 0.50 mm (average 0.10 mm).

Calcite and garnet were very minor constituents. Calcite occurred as anhedral patches between grains and garnet as tiny euhedral crystals.

Opaques were disseminated throughout the slide as anhedral grains, 0.05 to 0.75 mm, commonly with a rim of rutile.

SECTION C:

MINERALOGY:		MODAL ABUNDANCE (%)
1)	Quartz	40
2)	Microcline	10
3)	Plagioclase (andesine An_{43})	12
4)	Muscovite (inc. Sericite)	30
5)	Tourmaline (Dravite)	1
6)	Sphene	tr.
7)	Rutile	tr.
8)	Calcite	tr.
9)	Garnet	tr.
10)	Opaque	4

This section is very much the same as section D. More quartz and less microcline are present in this section.

The mineralogy is virtually identical except that sphene is present in section C. The average size of the sphene is 0.05 mm and it is usually rimmed by calcite.

SECTION D:

MINERALOGY:		MODAL ABUNDANCE (%)
1)	Quartz	30
2)	Microcline	20
3)	Plagioclase (labradorite An_{51})	15
4)	Muscovite (inc. Sericite)	30
5)	Tourmaline (Dravite)	1
6)	Calcite	tr.
7)	Rutile	tr.
8)	Garnet	tr.
9)	Opaque	2

This section shows a distinct banding of micaceous and quartzo-feldspathic minerals. The parallel alignment of the micas gives the slide a strong leipdoblastic texture. The size of the muscovite ranges from tiny euhedral crystals, less than 0.05 mm in length, to large patches of muscovite up to 2.0 mm in length (average 0.20 mm).

The grain size varied markedly within bands of the quartzo-feldspathic material. In some layers the average grain size was as low as 0.05 mm while in others the average size reached 0.20 mm. Individual grains varied from 0.01 to 0.50 mm. Sutured grain boundaries were common among the quartzo-feldspathic material but polygonal crystallization was also noted.

Porphyroblasts of quartz were abundant and ranged between 0.60 and 4.0 mm. Subgrains were present in the majority of the porphyroblasts and all the boundaries were sutured. Most of the porphyroblasts were weakly elongated parallel to the alignment of muscovite grains, which were often bent around the porphyroblasts. All quartz in this section displays strained extinction.

Some bands contain phenocrysts of plagioclase which have been heavily altered to sericite. The Michel-Levy test could not be effectively employed on these phenocrysts due to the amount of alteration. The mica that is present in these bands, other than the sericite, does not show the same preferred orientation that is present in the rest of the slide. It also shows mottled extinction and is commonly more altered than the mica in the rest of the section.

Subhedral crystals of tourmaline are aligned parallel to the muscovite outside the sericitic alteration zone. They vary between 0.20 and 1.0 mm in size. Garnet is present as very tiny euhedral crystals which are very rare. Calcite occurs as tiny patches within the sericitic alteration zone.

Rutile was identified in this slide. It occurs as a rim surrounding an opaque. A different opaque, without a rim of rutile, is more abundant. It is disseminated throughout the section as anhedral and subhedral grains ranging from 0.01 to 1.0 mm.

THIN SECTION D

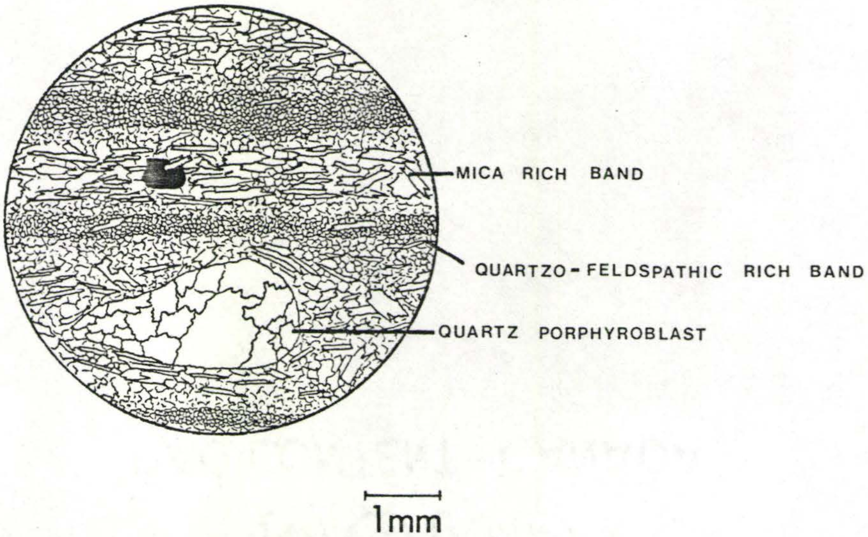

SECTION E:

MINERALOGY:	MODAL ABUNDANCE (%)
1) Quartz	34
2) Plagioclase (labradorite An_{64})	15
3) Microcline	3
4) Muscovite (inc. Sericite)	30
5) Biotite	3
6) Analcime	7
7) Heulandite	3
8) Sphene	1
9) Rutile	1
10) Calcite	tr.
11) Tourmaline (Dravite)	tr.
12) Spherulites	tr.
13) Opaque	2

There are two distinct zones in this section, one finely laminated and the other zeolitic.

The finely laminated zone has alternating bands, some rich in quartzo-feldspathic material and others rich in micas. The micas are aligned subparallel to one another and range between 0.02 and 0.70 mm in length (average 0.20 mm). The quartzo-feldspathic material commonly had sutured grain boundaries but polygonal crystallization was also noted. Grain size was variable among the quartz and the feldspar but the average size was 0.10 mm.

The zeolitic zone was dominated by anhedral patches and euhedral grains of analcime. The patches got as large as 4.0 mm but were often smaller. Euhedral crystals of heulandite, up to 0.60 mm, often occurred within the analcime. Phenocrysts of plagioclase, up to 2.5 mm in size, were also abundant in the zeolitic zone. The plagioclase has undergone extensive alteration to sericite.

Porphyroblasts of quartz were present in both zones of the slide. They ranged between 0.70 and 3.5 mm and commonly had subgrains with sutured boundaries.

Rutile was found throughout the slide, often rimming an opaque which may be ilmenite. The size of the opaque grains ranged between 0.01 and 0.50 mm. Sphene was also present in the section and was often associated with rutile. Anhedral grains of sphene, up to 0.40 mm in size, were always rimmed by calcite.

Minor subhedral grains of tourmaline occur in the well-banded area of the slide. They were aligned parallel to the mica and their average size was 0.10 mm.

Spherulites were a very minor constituent of this slide. They occurred on the boundary between the zeolitic zone and the well banded zone.

SECTION F:

MINERALOGY	MODAL ABUNDANCE (%)
1) Quartz	57
2) Microcline	30
3) Plagioclase (labradorite An_{52})	2
4) Barite	3
5) Biotite	2
6) Muscovite	1
7) Sphene	tr.
8) Rutile	tr.
9) Opaque	4

Quartz and feldspar are abundant in this section producing an overall mosaic texture. The average grain size of the quartzo-feldspathic material is 0.10 mm although local variation in size is common. Porphyroblasts of quartz, averaging 1.0 mm in size, are distributed throughout the slide. All of the quartz in the section exhibits strained extinction.

Biotite and muscovite, averaging 0.10 mm, occur subparallel to one another in the slide. The muscovite is generally less altered than the biotite.

Barite occurs as anhedral patches, 0.05 to 1.0 mm in size. The larger patches are made up of aggregates of grains.

Sphene and rutile are minor components. Tiny anhedral crystals of sphene occur throughout the slide. Rutile is commonly associated with an opaque, possibly ilmenite.

A second opaque in the slide, which is not rimmed by rutile, is far more common. It is scattered throughout the slide but appears to be preferentially concentrated in distinct bands. The anhedral and subhedral crystals range between 0.01 and 0.75 mm.

THIN SECTION F

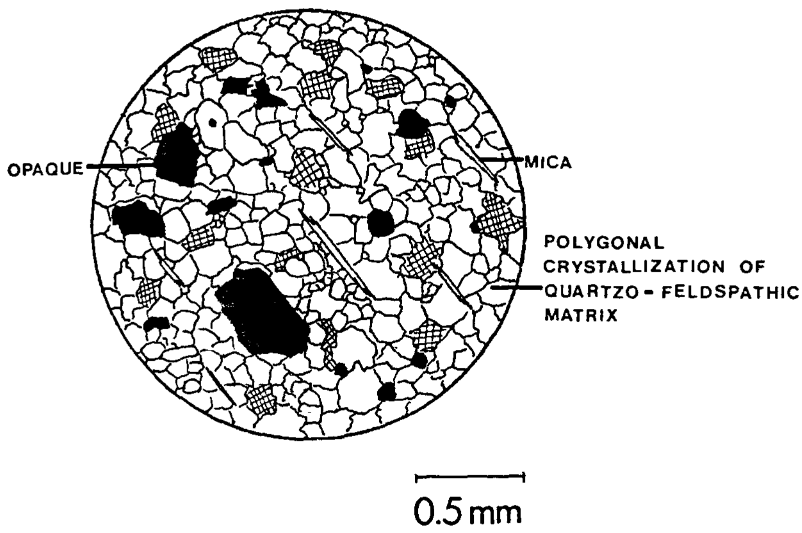

SECTION G:

MINERALOGY:	MODAL ABUNDANCE (%)
1) Quartz	25
2) Microcline	70
3) Sphene	tr.
4) Muscovite	tr.
5) Opaque	4

Quartz and microcline are the dominant minerals in this section. Their interlocking grain boundaries give the slide its distinct mosaic texture. The average grain size of the quartzo-feldspathic material is 0.10 mm.

Porphyroblasts of quartz, up to 3.0 mm in size are abundant. A majority of them have subgrains with sutured boundaries. All of the quartz in this section is strained.

Muscovite occurs as minute grains with no preferred orientation and averages 0.04 mm in length. It occurs interstitially in the quartzo-feldspathic material.

Sphene is a very minor constituent and individual crystals are about 0.02 mm in size. The grains are usually anhedral but some euhedral crystals were also noted.

The opaque mineral occurs as disseminated subhedral and euhedral grains throughout the slide; the size ranging between 0.01 and 1.0 mm.

SECTION H:

MINERALOGY:	MODAL ABUNDANCE (%)
1) Quartz	30
2) Microcline	50
3) Plagioclase (labradorite An_{56})	16
4) Muscovite	tr.
5) Sphene	tr.
6) Opaque	3

The majority of this section is quartzo-feldspathic material which gives the slide an overall mosaic texture. Grain size is variable from 0.02 to 0.50 mm (average 0.20 mm).

Porphyroblasts of quartz are abundant. They have numerous subgrains with weakly sutured boundaries and grain sizes up to 5.0 mm. All quartz in the section has strained extinction.

Phenocrysts of plagioclase, up to 2.0 mm, are also present. They commonly contain exsolution lamellae of microcline making them somewhat antiperthitic.

Muscovite and sphene were accessory minerals. Muscovite was identified as single euhedral crystals and as aggregates of crystals, never larger than 0.10 mm. Sphene occurred as rounded anhedral grains, averaging 0.04 mm.

Anhedral and subhedral opaques were disseminated throughout the section with grain sizes between 0.01 and 1.0 mm.

SECTION I:

MINERALOGY:	MODAL ABUNDANCE (%)
1) Quartz	20
2) Plagioclase	35
3) Microcline	10
4) Biotite	25
5) Muscovite	5
6) Calcite	4
7) Chlorite	tr.
8) Zircon	tr.

A strong foliation is evident in this section due to the subparallel alignment of biotite and muscovite. The euhedral biotite ranges from individual crystals smaller than 0.05 mm to aggregates of flakes up to 1.5 mm in length (average 0.40 mm), and commonly contains inclusions of zircon. Muscovite takes the same form as the biotite but is smaller, averaging 0.10 mm. Minor felted aggregates of chlorite occur with the biotite and average 0.15 mm in length.

The grain boundaries of the quartzo-feldspathic material are dominantly sutured but polygonal crystallization was also noted. Grain size varies from 0.025 to 0.75 mm (average 0.15 mm) with plagioclase slightly larger than the quartz and microcline on average. All quartz shows strained extinction.

Calcite occurs in anhedral patches, 0.02 to 1.5 mm, and may be an alteration of the plagioclase.

SECTION J:

MINERALOGY:	MODAL ABUNDANCE (%)
1) Quartz	24
2) Plagioclase (labradorite An_{62})	30
3) Microcline	24
4) Chlorite	10
5) Muscovite (inc. Sericite)	10
6) Calcite	1
7) Garnet	tr.
8) Sphene	tr.
9) Opaque	1

This section has a weak foliation due to the subparallel alignment of chlorite. It occurs as patches averaging 0.50 mm. The muscovite, varying between 0.02 and 0.75 mm, did not have any preferred grain orientation. It was also poorly crystallized, usually with ragged edges and often showing mottled extinction.

Sutured grain boundaries are common in the quartzo-feldspathic material but polygonal crystallization was observed as well. The average grain size of this material is 0.10 mm.

Phenocrysts of plagioclase are a major component, reaching 2.5 mm in size. They are anhedral and very patchy due to alteration to sericite and calcite.

Porphyroblasts of quartz, from 0.50 to 4.5 mm in size, are also abundant. All have subgrains with weakly sutured boundaries and inclusions of chlorite and muscovite are frequent.

Strained extinction was observed in all quartz in the section.

Sphene and garnet are present in trace amounts, sphene as anhedral grains less than 0.05 mm and garnet as smaller euhedral crystals.

Opaques were disseminated throughout the slide in subhedral grains, 0.02 to 0.50 mm.

THIN SECTION J

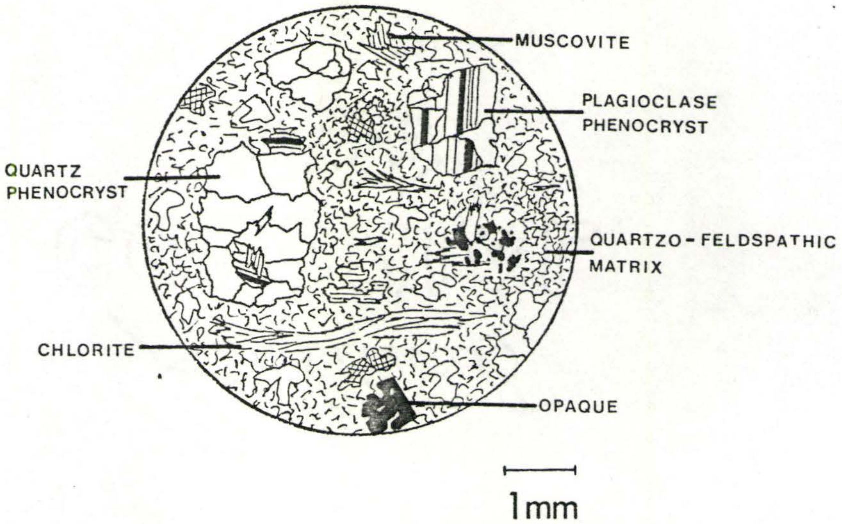

CORE #1:

MINERALOGY:	MODAL ABUNDANCE (%)
1) Quartz	35
2) Microcline	40
3) Muscovite	34
4) Opaque	1

This section consists of almost continuous layers of muscovite alternating with quartzo-feldspathic material. The muscovite shows a strong preferred orientation, although it frequently bends around porphyroblasts of quartz. The euhedral crystals vary from 0.05 to 1.5 mm (average 0.40 mm).

Polygonal crystallization is prominent in the quartzo-feldspathic material. Both the quartz and the microcline are anhedral and range between 0.05 and 0.25 mm (average 0.15 mm).

Porphyroblasts of quartz are present and are elongated parallel to the alignment of the muscovite. They reach 3.0 mm in length. Subgrains with strongly sutured boundaries are almost always present. All quartz in the section shows strained extinction.

Subhedral and euhedral opaques, 0.05 to 0.50 mm in size, are disseminated throughout the section.

THIN SECTION 1

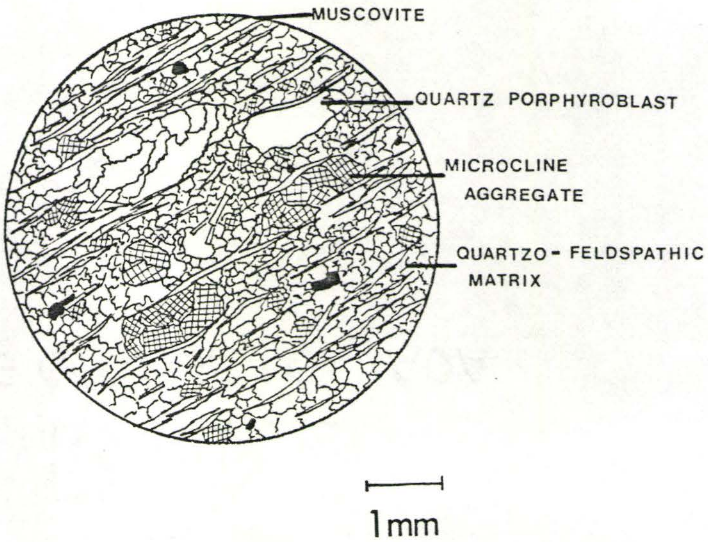

CORE #2:

MINERALOGY	MODAL ABUNDANCE (%)
1) Quartz	54
2) Microcline	2
3) Muscovite	40
4) Calcite	1
5) Tourmaline (Dravite)	1
6) Chlorite	tr.
7) Garnet	tr.
8) Opaque	1

This slide consists of alternating bands; some rich in muscovite and others rich in quartzo-feldspathic material. The euhedral to subhedral muscovite has a strong preferred orientation and commonly contains inclusions of quartz. The crystal length varies from 0.02 to 2.00 mm (average 0.5 mm).

Sutured grain boundaries are common in the quartzo-feldspathic material. The average grain size is 0.20 mm.

Porphyroblasts of quartz, up to 2.0 mm in size (average 1.0 mm), are present. They have subgrains with sutured boundaries and are elongated parallel to the foliation. All quartz in this section is strained.

Tourmaline and chlorite are oriented parallel to the muscovite. The subhedral tourmaline and the felted aggregates of chlorite range from 0.05 to 0.30 mm. Tourmaline sometimes occurs as an inclusion in muscovite.

Calcite occurs as discrete anhedral patches, as large as 0.70 mm, and is always associated with the muscovite. Garnet occurs as very tiny euhedral crystals.

Opaques are disseminated throughout the section and range from 0.04 to 0.50 mm.

THIN SECTION 2

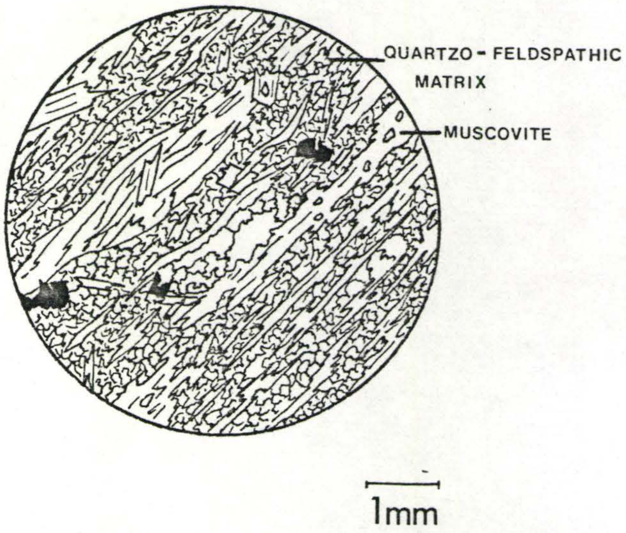

CORE #3A:

MINERALOGY:	MODAL ABUNDANCE (%)
1) Quartz	16
2) Microcline	70
3) Plagioclase (labradorite An_{32})	2
4) Biotite	5
5) Chlorite	3
6) Calcite	2
7) Muscovite (inc. Sericite)	tr.
8) Opaque	2

A weak foliation is evident in this section due to the subparallel alignment of biotite and chlorite. Euhedral crystals of biotite range from 0.02 to 0.50 mm (average 0.20 mm) while the felted aggregates of chlorite are as large as 4.0 mm (average 0.50 mm).

Grain size variation in the quartzo-feldspathic material is marked. Some areas of the section have an average grain size of 0.05 mm while others have average of 0.50 mm.

Minor porphyroblasts of quartz, up to 2.5 mm, were slightly elongated parallel to the alignment of the biotite and chlorite. Subgrains were noted in some of the porphyroblasts and they had weakly sutured boundaries. Strained extinction is present in all the quartz of the section.

Sericite was present as an alteration product of plagioclase. Calcite was present as interstitial patches.

Opaques were disseminated throughout the section but appeared to be concentrated in various bands. The anhedral to subhedral grains varied from 0.01 to 1.0 mm.

CORE #3B:

MINERALOGY	MODAL ABUNDANCE (%)
1) Quartz	10
2) Microcline	25
3) Plagioclose (labradorite An_{62})	15
4) Biotite	20
5) Muscovite (inc. Sericite)	15
6) Chlorite	3
7) Epidote	6
8) Calcite	5
9) Sphene	tr.
10) Zircon	tr.
11) Opaque	1

A weak foliation is present in the section due to the subparallel orientation of biotite and chlorite. The euhedral laths commonly occur as aggregates of flakes, averaging 0.25 mm.

Polygonal crystallization was observed in the quartzo-feldspathic material. The average grain size is 0.10 mm but local coarsening up to 0.50 mm is common.

Subhedral phenocrysts of plagioclase, up to 3.0 mm in size, are abundant. They have undergone extensive alteration to sericite, epidote and calcite.

Zircon is present as tiny inclusions in biotite. Sphene occurs as tiny anhedral and euhedral crystals, never larger than 0.05 mm. Opaques are a minor constituent, occurring as anhedral grains up to 0.20 mm.

CORE #4:

MINERALOGY:		MODAL ABUNDANCE (%)
1)	Quartz	43
2)	Microcline	37
3)	Plagioclase (Andesine An_{48})	3
4)	Muscovite	8
5)	Biotite	4
6)	Calcite	1
7)	Chlorite	tr.
8)	Tourmaline	tr.
9)	Zircon	tr.
10)	Barite	tr.
11)	Opaque	3

This section displays a leipdoblastic arrangement of muscovite, biotite, and chlorite. Individual euhedral crystals average 0.25 mm but clusters of grains get up to 2.0 mm. The presence of zircon is indicated by pleochroic halos in biotite.

Grain size variation is marked among the quartzo-feldspathic material giving the section a banded appearance. Sizes of the anhedral grains vary from an average of 0.05 mm in some bands to 0.50 mm in others. Polygonal crystallization was prominent in some bands but was missing in others.

Porphyroblasts of quartz, up to 3.0 mm in length, are abundant. They are commonly elongated parallel to the micas and always have subgrains with sutured boundaries. All of the quartz in this section shows strained extinction.

Calcite is present as anhedral patches up to 0.50 mm, but averaging 0.10 mm. Barite only occurs as one erratic patch measuring 1.25 mm in length. One subhedral crystal of tourmaline, 0.2 mm long, is also present.

Subhedral and euhedral opaques are disseminated throughout with grain size varying from 0.04 to 0.50 mm.

CORE #5

MINERALOGY:	MODAL ABUNDANCE (%)
1) Quartz	30
2) Microcline	59
3) Plagioclase (labradorite An_{50})	1
4) Biotite	2
5) Chlorite	3
6) Muscovite	1
7) Calcite	tr.
8) Barite	tr.
9) Garnet	tr.
10) Sphene	tr.
11) Opaque	3

The dominant texture in this section is the polygonal crystallization of the quartzo-feldspathic material. An average grain size is 0.10 mm but some bands and lenses of material are much coarser, averaging 0.40 mm. Microcline was often the dominant mineral in these coarser areas.

The platey minerals give the section a weak foloation due to their preferred orientation. Chlorite occurs in patches from 0.02 to 1.0 mm (average 0.25 mm). The biotite and muscovite have ragged edges and are often mottled. The average grain size for biotite is 0.10 mm and for muscovite is 0.075 mm.

Quartz porphyroblasts, as large as 4.0 mm (average 1.5 mm) are a major component. They are elongated parallel to the alignment of the platey minerals. The porphyroblasts have subgrains with weakly sutured boundaries and, along with the quartz in the groundmass, show strained extinction.

Calcite occurs as tiny patches in and around plagioclase. Barite also occurs as patches up to 0.25 mm in length. Garnet is a very minor constituent. Only one subhedral crystal, .10 mm in size, was identified.

Euhedral and subhedral opaques ranging betwen 0.01 and 1.0 mm are disseminated throughout the section.

APPENDIX 2

VALUES FOR WHOLE ROCK

ANALYSIS USING XRF

SAMPLE	SIO2	AL2O3	CAO	MGO	NA2O	K2O	FE2O3	MNO	TIO2	P2O5	LOI	SUM
C	66.5	16.4	2.93	2.06	2.10	3.77	2.41	0.01	0.28	0.10	3.08	99.7
D	65.8	17.4	3.05	1.61	2.23	5.09	1.88	0.01	0.29	0.11	2.39	99.9
G	72.9	13.3	0.03	0.05	0.45	11.2	0.74	0.00	0.17	0.02	0.77	99.7
F	73.3	11.1	0.01	0.13	0.50	8.78	1.21	0.00	0.21	0.04	1.39	96.8
A	69.9	15.8	2.32	1.28	2.55	3.94	1.82	0.02	0.28	0.10	1.70	99.8
B	66.8	16.0	2.66	1.74	3.36	2.85	3.45	0.03	0.51	0.24	1.39	99.3
H	68.2	15.0	0.06	0.03	3.41	8.84	2.57	0.00	0.20	0.03	1.85	100.2
I	61.1	15.4	3.59	3.25	5.26	3.04	5.07	0.07	0.63	0.42	2.16	100.2
J	67.9	17.0	0.88	1.17	7.16	2.20	1.79	0.02	0.25	0.10	1.47	100.0
CORE 1	68.6	18.1	0.00	0.35	1.03	8.69	0.74	0.00	0.32	0.03	1.93	99.9
CORE 2	71.7	15.6	0.26	0.91	0.23	5.52	1.94	0.00	0.30	0.14	2.62	99.3
CORE 3A	69.2	14.3	0.72	0.36	1.15	11.3	0.80	0.00	0.26	0.04	1.08	99.3
CORE 3B	61.7	16.6	4.47	1.70	4.61	2.88	5.01	0.05	0.68	0.20	1.70	99.8
CORE 4	68.0	15.9	0.09	0.23	1.50	10.9	0.89	0.00	0.27	0.03	0.93	98.9
CORE 5	72.8	12.4	0.24	0.17	1.17	9.47	1.91	0.01	0.24	0.09	0.77	99.3

BIBLIOGRAPHY

Baragar, W.R.A. and Irvine, T.N. 1971. A Guide to the Chemical Classification of theCommon Volcanic Rocks, Canadian Journal of Earth Sciences, V. 8. pp 523-544.

Barnett, E.S., Hutchinson, R.W., Adamcik, R.W., Barnett, R. 1982. Geology of the Agnico-Eagle Gold Deposit, Quebec. Precambrian Sulfide Deposits. GAC Spec. Paper 25. eds. R.W. Hutchinson, C.D. Spence, J.M. Franklin.

Bartley, M.W. and Page, T.W. 1957. A Geological Report on the Hemlo Area, Thunder Bay District, Ontario. Department of Industrial Development, Canadian Pacific Railway.

Berger, B.R. 1975. Determination of Metamorphic Grade for Two Formations of the Huronian Supergroup, Whitefish Falls Area, Ontario. B.Sc. Thesis. McMaster University, Hamilton, Ontario.

Berry, L.G. and Mason, B. 1959. Mineralogy. W.H. Freeman and Co., San Francisco.

Boles, J.R. 1977. Zeolites in Low-Grade Metamorphic Grades. Mineralogy and Geology of Natural Zeolites. Min. Soc. Am. Short Course Notes, V.4. ed. F.A. Mumpton. Washington, D.C.

Boyle, R.W. 1980. Gold Deposits: A Review of Their Geological and Geochemical Setting. Geology of Canadian Gold Deposits. Can. Inst. Min. Metal. Spec. V. 24. pp.1-5.

Church, T.M. 1979. Marine Barite. Marine Minerals. Min. Soc. Am. Short Course Notes, V. 6. ed. R.G. Burns. Washington, D.C. pp 175-209.

Crockett, J.H. 1978. Gold: Abundance in Common Rocks. Handbook of Geochemistry, V. 2/5. ed. K.H. Wedepohl. Springer-Verlag, Berlin.

Debicki, E.J. 1971. Fragment-Matrix Chemical Analysis of Keewatin Felsic Volcanics From the Kakagi Lake Area, N.W. Ontario. M.Sc. Thesis. McMaster University, Hamilton, Ontario.

Deer, W.A., Howie, R.A. and Zussman, J. 1966. An Introduction to the Rock Forming Minerals. Longman Group Ltd., London.

Dott Jr., R.H. and Batten, R.L. 1981. Evolution of the Earth, 3rd ed. McGraw-Hill, New York.

Fryer, B.J., Kerrich, R., Hutchinson, R.W., Peirce, M.G. and Rogers, D.S. 1979. Archean Precious-Metal Hydrothermal Systems, Dome Mine, ABitibi Greenstone Belt. 1. Patterns of Alteration and Metal Distribution. Can. Jour. Earth Sci., V.16., pp 421-439.

Goodwin, A.M. 1977. Archean Volcanism in Superior Province, Canadian Shield. GAC Spec. Paper 16, eds. W.R.A. Baragar, L.C. Coleman, J.M. Hall. pp. 205-241.

Hobbs, B.E., Means, W.E. and Williams, P.F. 1976. An Outline of Structural Geology. John Wiley and Sons, New York.

Hodgson, C.J. and MacGeehan, P.J. 1980. A Review of the Geological Characteristics of 'Gold-Only' Deposits in the Superior Province of the Canadian Shield. Geology of Canadian Gold Deposits. Can. Inst. Min. Metal., Spec. V. 24.

Hutchinson, C.S. 1974. Laboratory Handbook of Petrographic Techniques. John Wiley and Sons, New York.

Hyndman, D.W. 1972. Petrology of Igneous and Metamorphic Rocks. McGraw Hill Inc., New York.

Jensen, L.S. 1976. A New Cation Plot for Classifying Sub-alkalic Volcanic Rocks. Ont. Div. Mines Misc. Pap. 66, 22 p.

Karvinen, W.O. 1981. Geology and Evolution of Gold Deposits, Timmins Area, Ontario. Genesis of Archean Volcanic-Hosted Gold Deposits. O.G.S. Misc. Pap. 97. eds. E.G. Pye and R.G. Roberts. pp. 29-46.

Kerr, P.F. 1977. Optical Mineralogy, 4th ed. McGraw Hill Inc., New York.

Mineral Powder Diffraction File: Search Manual. 1980. Joint Committee on Powder Diffraction Standards. International Centre for Diffraction Data. Swarthmore, Pa.

Muir, T.L. 1982. Geology of the Hemlo Area. O.G.S. Report 217. 65 p.

Phillips, W.R. 1971. Mineral Optics: Principles and Techniques. W.H. Freeman and Co., San Francisco.

Selected Powder Diffraction Data for Minerals, 1st Edition. 1974. Joint Committee on Powder Diffraction Standards. International Centre for Diffraction Data. Swarthmore, Pa.

Spry, Alan 1979. Metamorphic Textures. Pergamon Press, Oxford.

Valliant, R.I. and Hutchinson, R.W. 1980a. Stratigraphic Distribution and Genesis of Gold Deposits, Bousquet Region, Northwest Quebec. Geology of Canadian Gold Deposits. Can. Inst. Min. Metal. Spec. V. 24. pp. 27-40.

Valliant, R.I., Mongeau, C. and Doucet, R. 1980b. The Bousquet Pyritic Gold Deposit, Bousquet Region, Quebec: Descriptive Geology and Preliminary Interpretations on Genesis. Geology of Canadian Gold Deposits. Can. Ins. Min. Metal. Spec. V. 24. pp. 41-49.

Winkler, H.G.F. 1979. Petrogenesis of Metamorphic Rocks, 5th ed. Springer-Verlag, Berlin.

Wolff, J.M. 1977. The Geochemical Nature of an Archean Plutonic-Volcanic Suite as Exemplified by the Kakagi-Stephen Lakes Area, N.W. Ontario. M.Sc. Thesis, McMaster University, Hamilton, Ontario.